

Original Research

Core Ideas

- 3D time-lapse ERT is used to monitor water infiltration for mining environmental issues.
- Geoelectrical images provide information where no hydrogeological data is available.
- Water resistivity must be taken into account to understand bulk resistivity variations.
- Electrical resistivity of water is used as a tracer to reconstruct water infiltration.
- Infiltration model integrating both hydrogeological and geophysical data is proposed.

A. Dimech, M. Chouteau, M. Aubertin, and V. Martin, École Polytechnique de Montréal, Montréal, QC H3T 1J4, Canada; B. Bussière and B. Plante, Univ. du Québec en Abitibi-Témiscamingue (UQAT), Rouyn-Noranda, QC J9X 5E4, Canada; A. Dimech, M. Chouteau, M. Aubertin, B. Bussière, V. Martin, and B. Plante, Research Institute on Mines and Environment (RIME), UQAT-Polytechnique, Montreal, QC H3C 3A7, Canada. *Corresponding author (adrien.dimech@gmail.com).

Received 4 May 2018.
Accepted 24 Jan. 2019.

Citation: Dimech, A., M. Chouteau, M. Aubertin, B. Bussière, V. Martin, and B. Plante. 2019. Three-dimensional time-lapse geoelectrical monitoring of water infiltration in an experimental mine waste rock pile. *Vadose Zone J.* 18:180098. doi:10.2136/vzj2018.05.0098

© 2019 The Author(s). This is an open access article distributed under the CC BY-NC-ND license (<http://creativecommons.org/licenses/by-nc-nd/4.0/>).

Three-Dimensional Time-Lapse Geoelectrical Monitoring of Water Infiltration in an Experimental Mine Waste Rock Pile

Adrien Dimech*, Michel Chouteau, Michel Aubertin, Bruno Bussière, Vincent Martin, and Benoît Plante

Open-pit mines often generate large quantities of waste rocks that are usually stored in waste rock piles (WRPs). When the waste rocks contain reactive minerals (mainly sulfides), water and air circulation can lead to the generation of contaminated drainage. An experimental WRP was built at the Lac Tio mine (Canada) to validate a new disposal method that aims to limit water infiltration into reactive waste rocks. More specifically, a flow control layer was placed on top of the pile, which represents a typical bench level, to divert water toward the outer edge. Hydrogeological sensors and geophysical electrodes were installed for monitoring moisture distribution in the pile during infiltration events. A three-dimensional (3D) time-lapse hydrogeophysical monitoring program was conducted to assess water infiltration and movement. Readings from the 192 circular electrodes buried in the WRP were used to reconstruct the 3D bulk electrical resistivity (ER) variations over time. A significant effort was devoted to assessing the spatiotemporal evolution of water ER because the bulk ER is strongly affected by water quality (and content). The water ER was used as a tracer to monitor the infiltration and flow of resistive and conductive waters. The results indicate that the inclined surface layer efficiently diverts a large part of the added water away from the core of the pile. Local and global models of water infiltration explaining both bulk and water ER variations are proposed. The results shown here are consistent with hydrogeological data and provide additional insights to characterize the behavior of the pile.

Abbreviations: 2D, two-dimensional; 3D, three-dimensional; ER, electrical resistivity; ERT, electrical resistivity tomography; FCL, flow control layer; VWC, volumetric water content; WRP, waste rock pile.

Waste rocks with no economic value are extracted to access the ore in a mine and are usually stored in surface piles. These WRPs can exceed 300 m in height and contain up to several hundred million cubic meters of waste rocks (Aubertin et al., 2002; McCarter, 1990; McLemore et al., 2009; Morin, 1990). Reactive minerals in the waste rocks may oxidize and generate contaminated mine drainage when these large deposits are exposed to air and water flows. Eventually, metal concentrations in the effluent can exceed regulation levels, and this may require costly water treatment at the mine site (Bussière et al., 2005). A few solutions have been proposed to address this type of environmental issue, mainly by controlling water infiltration in the reactive waste rocks. One promising option is to use the layered internal structure of piles to limit deep-water infiltration following precipitation on the pile surface (Aubertin et al., 2002, 2005). Numerical analyses have shown that the capillary barrier effect created by the superposition of an inclined fine-grained material layer over coarser waste rock tends to divert water toward the edge of the pile containing non- or less-reactive waste rocks (Fala et al., 2003, 2005; Molson et al., 2005). Flow control layers (FCLs) made of compacted (crushed) nonreactive waste rocks may prevent water from being in contact with reactive minerals (mainly sulfides) in the WRP, thus limiting contaminated drainage generation in the long term. This technique can be integrated directly into mine operations since the repeated passages of heavy machinery on

the surface naturally create the required fine-grained, compacted layers (Martin et al., 2006). Such layers can also be added in a controlled manner as part of the construction process. The superposition of several FCL in a large pile may significantly reduce moisture content and water flow in the reactive core of the piles as illustrated in Fig. 1 (Aubertin et al., 2005). The efficiency of FCL for limiting water infiltration in WRP piles has been evaluated through several unsaturated water flow simulations (Aubertin et al., 2009; Broda et al., 2013, 2014, 2017; Dawood et al., 2011; Fala et al., 2003, 2006; Martin et al., 2004). However, it is necessary to validate the FCL efficiency under field conditions. This can be accomplished by monitoring the actual hydrogeological behavior of an experimental and instrumented pilot-scale WRP with a FCL (Martin et al., 2017). Such hydrogeological monitoring is expected to provide relevant datasets to validate and optimize the FCL concept for future reclamation of existing WRPs (Bussière et al., 2015).

Most of the studies that involve monitoring of the hydrogeological behavior of pilot-scale sites under field conditions use traditional point measurement sensors (Amos et al., 2015; Smith et al., 2013). However, these sensors (moisture and suction probes for instance) might not be suitable for large-scale monitoring of heterogeneous media since they can be challenging to install and only provide measurements in a small volume of medium; it is thus necessary to use many of them to cover large volumes (e.g., Binley et al., 2010, 2015). Moreover, it is usually difficult to monitor sites with large blocks or high level of compaction (such as waste rock piles and landfill liners) because these sensors are relatively

fragile (Audebert et al., 2016a, 2016b). In addition, the medium surrounding sensors can be modified through their placement so measurements may not be entirely representative of the actual system (Grellier et al., 2006; Hübner et al., 2017).

For these reasons, it might be advantageous to complement traditional hydrogeological monitoring techniques with hydrogeophysical methods that are usually noninvasive and cost-effective and which enable large-scale volumetric measurements of physical parameters correlated with hydrogeological characteristics (such as volumetric water content and water quality) (Binley et al., 2010, 2015; Koestel et al., 2008, 2009; Robinson et al., 2008). Electrical resistivity tomography (ERT) is particularly suitable for hydrogeological applications since ERT can provide high-resolution (spatial and temporal) monitoring of the bulk ER distribution (two and three dimensional), which is directly linked to volumetric water content and ionic solute concentration (Archie, 1942; Attia et al., 2008; Binley et al., 2015; Loke et al., 2013; Singha et al., 2015; Singha and Gorelick, 2005).

Various applications of the ERT method have been presented over the past two decades for: hydrogeological studies (Clément et al., 2014; Hübner et al., 2017, 2015; Nimmer et al., 2008), agricultural applications (Cassiani et al., 2012; Michot et al., 2003; Uhlemann et al., 2016b), ground water resources (Binley et al., 2002; Kuras et al., 2009), tracer and contaminant plume monitoring (Audebert et al., 2016a, 2016b; Koestel et al., 2009, 2008; Kuras et al., 2016, 2014; Power et al., 2014; Rucker et al., 2011; Wilkinson et al., 2010), geotechnical applications (Chambers et

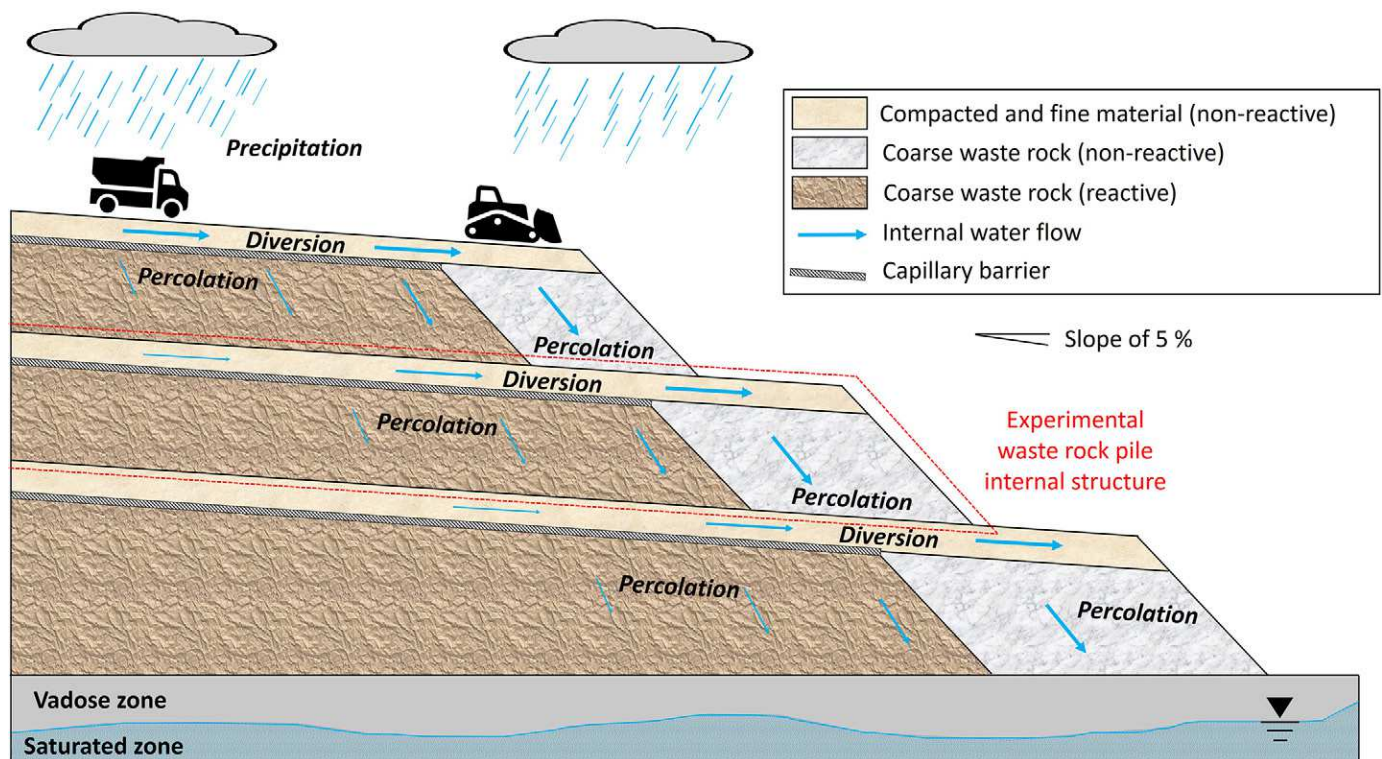


Fig. 1. Internal structure of the pile showing compacted and inclined layers, made from sandy materials (such as crushed waste rocks), diverting water away from the reactive core to limit contaminated drainage generation. Adapted from Aubertin et al. (2005) and Aubertin (2013).

al., 2014, 2015; Uhlemann et al., 2016a, 2017) and mining environmental issues (Anterrieu et al., 2010; Dimech, 2018; Dimech et al., 2018, 2017; Intissar, 2009; Power et al., 2018).

Recent developments of the ERT method over the past decade have increased the spatial and temporal resolution for hydrogeological processes monitoring, with optimization of measurement protocols using several hundreds of electrodes (Loke et al., 2014a, 2014b, 2015a, 2015b; Uhlemann et al., 2018; Wilkinson et al., 2012) and with two-, three-, and four-dimensional inversion software (Günther et al., 2006; Johnson et al., 2017, 2010; Rucker et al., 2017, 2006). Moreover, new approaches have been developed to integrate geophysical monitoring results into hydrogeological modeling to complement traditional hydrogeological monitoring techniques for laboratory experiments or field scale studies (Binley et al., 2002; Chou et al., 2016; Dawood et al., 2011; Kemna et al., 2002; Koestel et al., 2008, 2009; Robinson et al., 2009). Finally, recent developments of semi-autonomous or fully autonomous acquisition systems have made possible continuous geoelectrical monitoring of hydrogeological processes, for coastal aquifers (Kuras et al., 2009; Ogilvy et al., 2009) or landslides applications for example (Gunn et al., 2013; Uhlemann et al., 2016a, 2017).

Despite these recent successful applications, qualitative and quantitative interpretation of ERT datasets in terms of hydrogeological properties remain very challenging, especially when both moisture content and groundwater ionic content may change simultaneously (Kemna et al., 2002; Koestel et al., 2008; Singha and Gorelick, 2005). This issue has been addressed for laboratory studies where one (or several) physical parameters can be controlled and the medium is usually homogeneous (Bechtold et al., 2012; Binley et al., 1996; Garré et al., 2010; Koestel et al., 2008; Kremer et al., 2018; Slater et al., 2000). Large-scale field studies usually assume that either solute conductivity or volumetric water content is constant over time to provide quantitative hydrogeological results by using empirical or laboratory petrophysical relationships (Clément et al., 2014; Dimech et al., 2018; Dumont et al., 2018; Hübner et al., 2017; Jayawickreme et al., 2008; Kuras et al., 2009; Uhlemann et al., 2017). However, these hypotheses may not be applicable for some media where both water content and quality change during hydrogeological processes, such as for landfills and WRPs. These media can be highly heterogeneous, with high variations of degree of compaction, and often have a complex hydrogeological behavior (Audebert et al., 2016a, 2016b; Blackmore et al., 2018; Lahmira et al., 2017). Hydrogeological processes (such as precipitations, recharge and water percolation) can also induce great variations of water conductivity when the media is highly conductive and the pore water shows highly variable ionic concentrations (Audebert et al., 2016a; Plante et al., 2014).

Several models describing the relationship between bulk ER, volumetric water content and ionic concentrations have been proposed over the past 50 yr (e.g., Archie, 1942; Attia et al., 2008; Binley et al., 2015). Some of these models are commonly used to convert a change in bulk ER obtained by ERT monitoring into a change in volumetric water content, thus providing a large-scale

temporal evaluation of volumetric water content for diverse applications (e.g., Anterrieu et al., 2010; Bechtold et al., 2012; Singha et al., 2015). However, most quantitative applications of ERT monitoring assume that the fluid nature (i.e., water ER, or ionic concentration) does not change over time in the medium, which is not necessarily the case in practice (Singha et al., 2015; Singha and Gorelick, 2005).

The aim of this study was to monitor water infiltration in an experimental WRP during a controlled infiltration event. Both traditional point-measurement hydrogeological sensors and geophysical monitoring were used in the field to evaluate the hydrogeological behavior of an inclined FCL made of compacted sand placed on the waste rocks. The capillary barrier effect developed between the compacted sand layer and the coarse waste rock underneath was expected to laterally divert part of the infiltrated water. This study focuses on the results of an ERT survey performed in 2017 and on the temporal and spatial distributions of both bulk and water ER in the pile. The geophysical data are expected to reflect the variations of bulk ER induced by water infiltration (i.e., variations of volumetric water content in the pile and of ionic concentrations in the infiltrated water) and thus provide qualitative and quantitative data describing hydrogeological processes in the WRP to complement point-sensors. The major objectives of this research work were (i) to assess the applicability of geoelectrical monitoring to image water infiltration in mine WRPs and (ii) to use geoelectrical monitoring to provide information describing water infiltration to complement traditional point-measurement monitoring techniques.

Materials and Methods

Site Description

The Lac Tio mine located north of Havre-St-Pierre (Quebec, Canada) is an open-pit mine producing iron and titanium from a large hemo-ilmenite deposit. It has been in operation since 1950. The mining activities have generated ~72 Tg of waste rocks stored in piles covering an area of ~130 ha (WSP Canada, 2014). Two main types of waste rocks are generated: one made of anorthosite and the other with hemo-ilmenite mineralization with a cut-off grade of 76% (WSP Canada, 2014). The Lac Tio mine anorthosite waste rock is considered nonreactive because its sulfide content is very low and it does not generate contaminants (Plante et al., 2010). The relatively small amounts of sulfides contained in the hemo-ilmenite waste rock (mainly pyrite) can be oxidized by water and air. The reactions can then produce contaminated neutral drainage, which may be responsible for occasional nickel leaching in the drainage water around the base of the waste rock piles (Bussière et al., 2015; Plante et al., 2011a, 2011b, 2014).

An experimental WRP was built at the Lac Tio mine in 2014 and 2015 to study the hydrogeological behavior of a FCL under field conditions at a pilot scale. Compacted layers of sand (60 cm thick) and nonreactive crushed waste rock (25 cm thick) were placed on top of the 60-m-long, 7-m-high (at the top), and

30-m-wide (at the base) WRP. The superposition of the compacted sand layer on the coarser waste rock was expected to create a capillary barrier effect that could limit deep water infiltration (Aubertin et al., 2002, 2009; Bréard-Lanoix, 2017; Fala et al., 2003, 2005). Numerical simulations indicated that this FCL, inclined with a slope of 5%, could decrease infiltration in the experimental pile by up to 90%, particularly upslope (Broda et al., 2017). To validate the FCL concept and evaluate the accuracy of numerical model simulations, hydrogeological and geochemical monitoring of the pile was performed. The experimental WRP was built to reflect the internal structure of existing piles using dozers and trucks. The grain size of the waste rock varies from fine particles (silty size particles) to blocks (smaller than ~60 cm). Construction naturally produced high heterogeneity that makes it challenging to evaluate hydrogeological behavior of such a WRP (Aubertin et al., 2008; Blackmore et al., 2018; Martin et al., 2006).

The experimental WRP constructed on the site of the Lac Tio mine was instrumented with both hydrogeological and geophysical sensors to monitor water infiltration and movement over time (Dimech et al., 2017, 2018; Dubuc et al., 2017; Martin et al., 2017). The geometry of the pile and the instrument location are shown in Fig. 2. Figure 2a presents a longitudinal, two-dimensional (2D) slice in the center of the WRP, while Fig. 2b details a transversal 2D slice where probes are located (without the inclined side edges). Moisture content probes (42 GS3; Decagon Devices, 2016) were positioned near the surface of the pile, above and below the FCL interface (30 sensors), and close to its base (12 sensors). These sensors measure temperature, bulk ER, and volumetric water content and were calibrated in the laboratory with samples from the experimental WRP (Dubuc, 2018; Dubuc et al., 2017). Suction probes (24 MPS-2; Decagon Devices, 2017) were positioned near the interface between the FCL and waste rock (12 sensors) and the base of the pile (12 sensors) to monitor temperature and (negative) pore water pressure. In addition, six lysimeters constructed at the bottom of the pile were used to collect percolating waters for geochemical analyses of the leachates (Martin et al., 2017; Poaty et al., 2018) and were connected to flow meters that measured

exfiltration flow rates (Dubuc et al., 2017). In addition, over 1000 m of fiber optic cable were installed near the surface and the base of the pile to provide a distributed measure of the temperature in the pile (Broda et al., 2013b). It would have been difficult (and hazardous) to instrument the core of the pile with classical hydrogeological sensors because of the construction method used (push dumping), the nature of the waste rock (with large blocks), and the risks involved (for the personnel and equipment). To help overcome this limitation, 192 cylindrical electrodes (1 cm thick, 10 cm diam.) were positioned in the FCL (96 electrodes) and in the sand layer at the base of the pile (96 electrodes) (Dimech et al., 2017). These two regular electrodes grids of four by 24 electrodes, with a spacing of 2 m by 2 m, allowed ER monitoring of the entire pile over time. Electrode locations are shown in Fig. 2 with black dots for the longitudinal (Fig. 2a) and transversal sections (Fig. 2b) of the pile.

Methodology

A dedicated geoelectrical monitoring system was designed to conduct ERT imaging of the experimental pile with the 192 buried electrodes shown in Fig. 3. The Terrameter LS (ABEM Instrument, 2016) was used to apply current and measure potential according to specific measurement protocols. Two switch boxes ES1064C were used to connect the 192 electrodes with specific connection boxes. As illustrated in Fig. 3, 175 electrodes (black dots) were used. Optimized protocol was designed for the field survey conducted in summer 2017. This protocol (involving 1000 quadrupoles in 1 h) was defined following the approach of Stummer et al. (2004), Wilkinson et al. (2010, 2012) and Loke et al. (2014a, 2014b, 2015a). The sensitivity of the protocol (i.e., impact of each elementary volume of the pile on the electrical response) is shown in Fig. 3b. The isosensitivity surfaces in this figure show areas where geophysical monitoring is expected to have satisfying resolution and where the reconstruction of ER distribution after inversion is assumed to be the most reliable. Both spatial and temporal resolution were improved by the optimized protocol vs. other more standard protocols (Wenner Schlumberger and

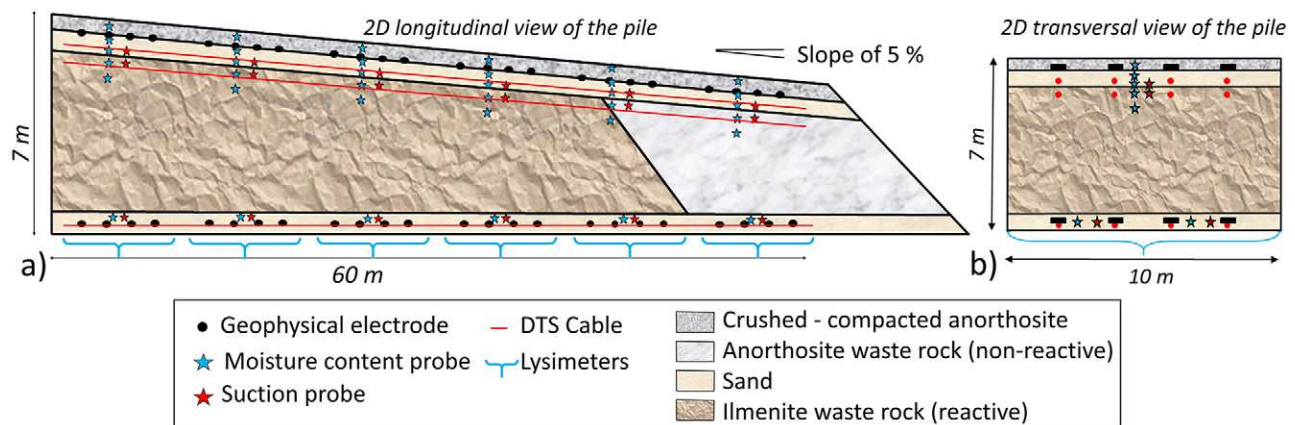
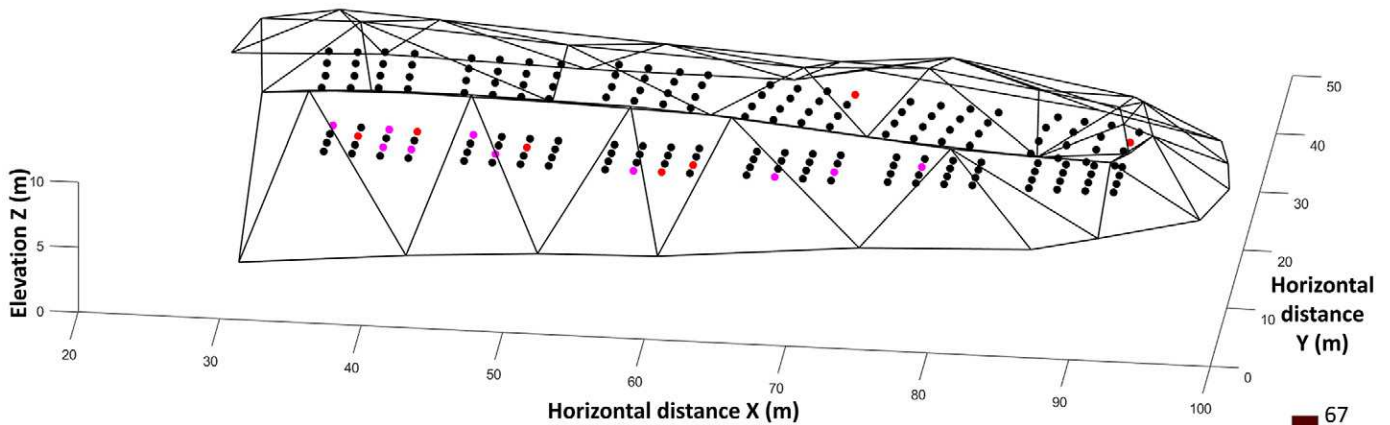


Fig. 2. Two-dimensional sections of the experimental waste rock pile (WRP) at the Lac Tio mine showing the internal structure and instrumentation (hydrogeological and geophysical). Not to scale (from Dimech et al., 2017).

a) 3D visualization of the geometry of the experimental waste rock pile with the electrode distribution



b) Sensitivity of the optimized protocol used in summer 2017 (1000 configurations : 1 hour)

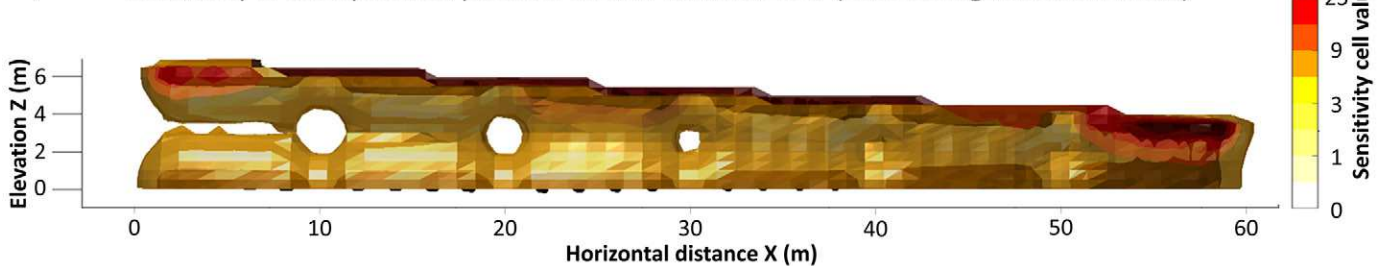


Fig. 3. (a) Three-dimensional view of the geometry of the experimental waste rock pile (WRP) with electrode positions, with black dots corresponding to operational electrodes (175/192) and pink and red dots indicating dysfunctional electrodes (17/192) and (b) geoelectrical sensitivities of the optimized protocol used in summer 2017.

dipole–dipole) used in Fall 2016 (see Dimech et al. [2017] for more details on the survey performed in 2016).

Recent ERT inversion software allows reconstructing subsurface electrical resistivity distribution for complex geometries by using 3D tetrahedral meshes (Günther et al., 2006; Johnson et al., 2010, 2017; Rücker et al., 2006, 2017). It may be more suitable to use 3D tetrahedral meshes when the geometry of the survey site is complex and produces artifacts from classical inversions (as detailed in Dimech et al. [2017] for the Lac Tio experimental pile). Several surveys were performed during the construction of the experimental WRP to measure the exact geometry of the different layers and assess the exact position of the instrumentation. As a result, a 3D tetrahedron numerical model of the pile with 400,000 elements was generated including internal geometry, sensor positions and external topography with high resolution (centimetric resolution accuracy) (Fig. 4). This precise modeling of the pile led to more refined time-lapse inversions of the 3D geoelectrical dataset performed with the software E4D (Johnson et al., 2010). For example, sharp electrical resistivity variations were allowed at the interface between ilmenite and anorthosite, while a spatial smoothing was imposed within the sand layer and the ilmenite waste rocks. The additional information about the inner structure of the experimental WRP was expected to improve the quality of the results.

Both hydrogeological and geophysical monitoring of the pile seek to image water infiltration and flow in the pile after recharge.

Hydrogeological sensors monitored the pile continuously with measurements made every 2 h. Geophysical measurements could only be recorded when the research team was on site (lack of power and no internet access). Several artificial precipitation events were performed with a water truck to simulate relatively large precipitations of short duration (Bussière et al., 2015; Dimech et al., 2017, 2018; Dubuc et al., 2017; Martin et al., 2017). The results presented here focus on the monitoring of a large-scale artificial precipitation event performed on 7 June 2017. Approximately 28 m³ of conductive water (water ER of $\rho_w \approx 10 \Omega \text{ m}$, corresponding to an electrical conductivity $EC \approx 1000 \mu\text{S cm}^{-1}$) was sprayed evenly on top of the pile with a water tanker truck during ~10 h, simulating a 47-mm recharge event. The wetting rate was measured and controlled to minimize runoff at the surface of the pile as described by Dubuc et al. (2017). The actual volume of water sprinkled on top of the pile was measured at different locations (Dubuc, 2018; Dubuc et al., 2017). Water samples were collected from the lysimeters at the base for geochemical analyses of the leachate (Poaty et al., 2018).

The initial geoelectrical database was analyzed to exclude quadrupoles with high measurement errors: the thresholds used for reciprocity errors and variances on the measured potentials were respectively 10 and 5% and the number of stacking ranged between 2 and 3. Reciprocal data were measured before and after the infiltration event to improve the temporal resolution during water infiltration. Three-dimensional, time-lapse inversions were performed with E4D

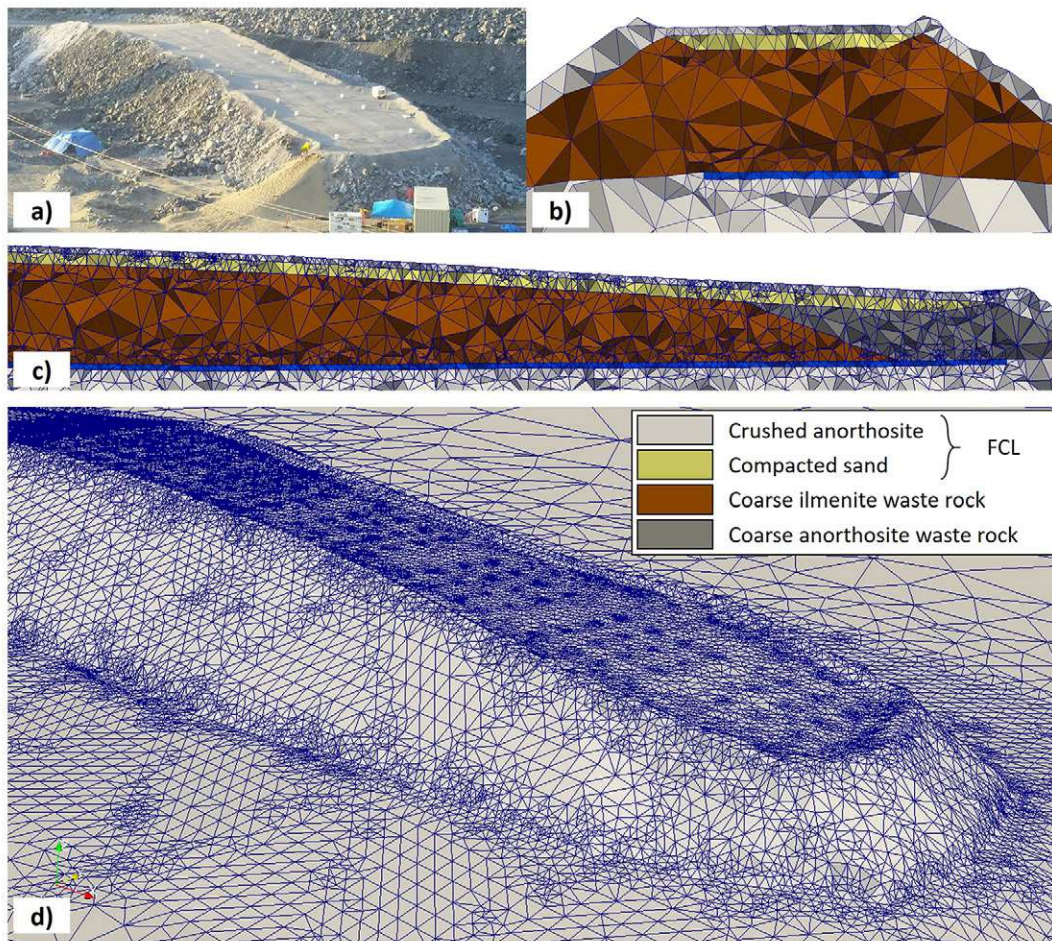


Fig. 4. (a) Photograph of the experimental waste rock pile (WRP) and views of the 3D numerical model; (b) transversal and (c) longitudinal sections and (d) 3D rendering of the external geometry of the experimental waste rock pile. The flow control layer (FCL) is made of crushed anorthosite (light gray) and compacted sand (yellow). The waste rock pile is made of coarse ilmenite waste rocks (brown) and coarse anorthosite waste rocks (dark gray).

(Johnson et al., 2010) to obtain a resistivity model of the WRP every hour and a total of 240 3D images were generated.

Results

Three-Dimensional Time-Lapse Inverted Distribution of Bulk Electrical Resistivity

Three-Dimensional Inverted Images of the Pile before and after Infiltration

Results of 3D time-lapse inversions are presented with two types of graphics: Fig. 5 presents longitudinal and transversal sections of the 3D inverted model showing the bulk ER distribution before and after the infiltration event (6 and 9 June); Fig. 6 displays six 1D vertical profiles of bulk ER extracted from the 3D inverted model along the longitudinal axis of the pile at three different dates (6, 8, and 13 June). The diagrams on the left of the profiles show the structure and the geometry of the pile at these locations based on the surveys performed during the pile construction. The inverse model is considered representative of the actual state of the pile with a global error as low as 2.5%. However, since

the resolution is lower in the center of the pile because of larger electrode spacing (cf. Fig. 3b), the deviation between image ER and actual ER might exceed 2.5%

The FCL at the top of the pile, made of a sand layer (beneath protective crushed waste rocks), was initially resistive (between 1000 and 4000 Ω m). The downslope end of the pile made of coarse anorthosite waste rocks (50 m < x < 60 m) was highly resistive (>4000 Ω m) and the core of the pile composed of mineralized ilmenite waste rocks was more conductive (between 60 and 1000 Ω m) as shown by Fig. 5 and the black line on Fig. 6. By comparing the images obtained before and after water infiltration, it became possible to identify the areas where ER values were the most affected by the infiltration event. Globally, the FCL at the surface (gray and yellow materials on Fig. 6) became more conductive because of water infiltration, with ER values dropping from a range of 1000 to 4000 Ω m to a range of 400 to 2000 Ω m. The ER values in the FCL remained low 6 d after the infiltration event as shown by the cyan lines in Fig. 6. Unlike the FCL, ilmenite waste rock (brown material in Fig. 6) became somewhat more resistive after water infiltration, with bulk ER values ranging from 60 to

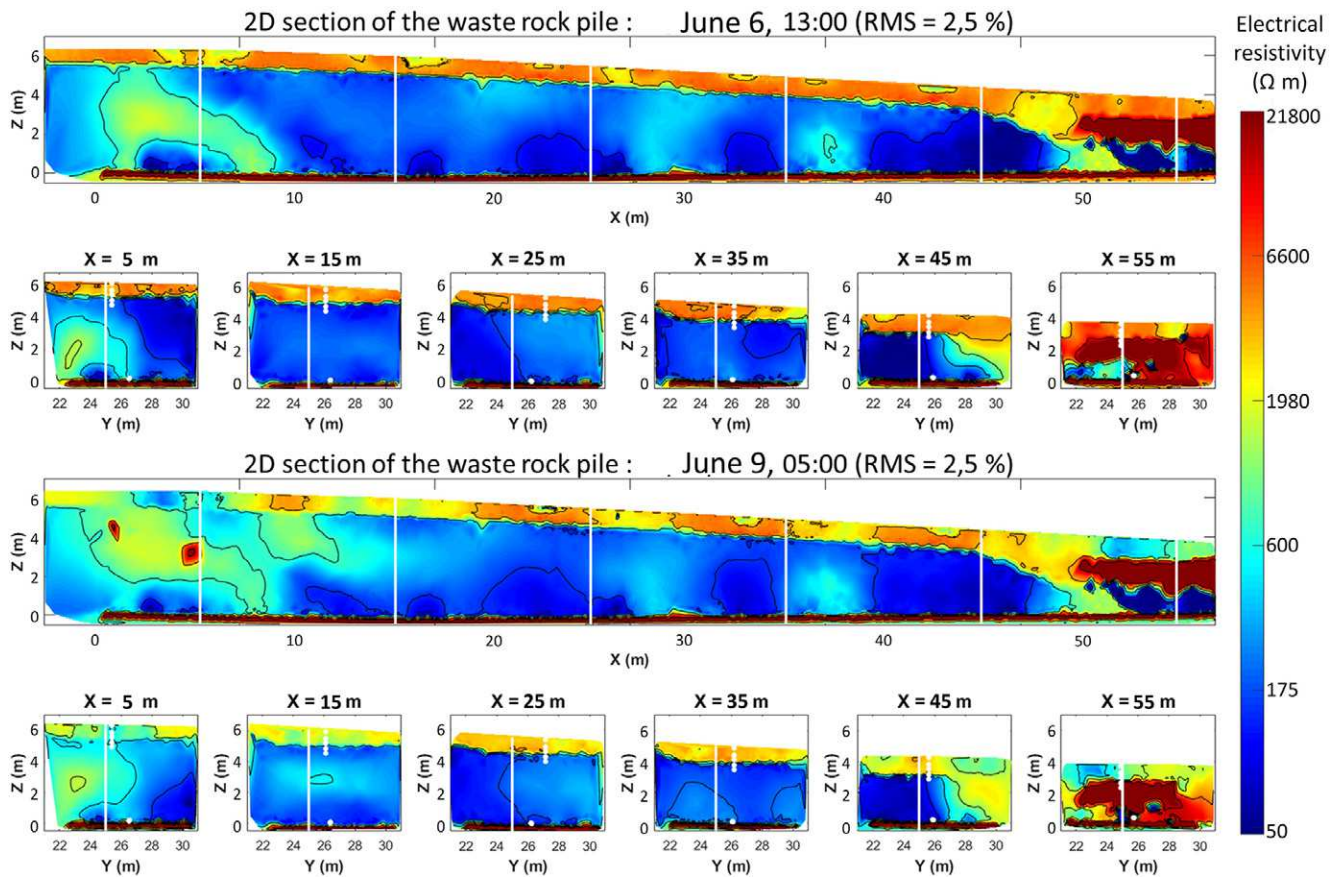


Fig. 5. Three-dimensional distribution of the electrical resistivity (ER) in the experimental waste rock pile (WRP) before (6 June 2017) and after (9 June 2017) the infiltration test. The results are presented for 2D sections of the pile (longitudinal and transversal) extracted from the 3D time-lapse distribution of resistivity.

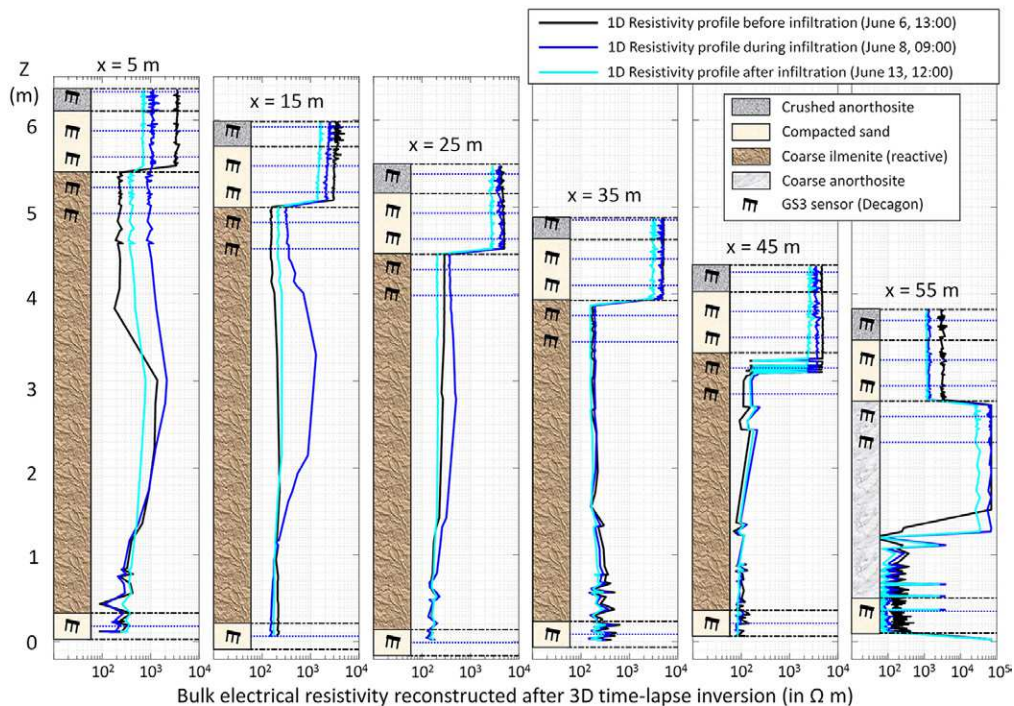


Fig. 6. One-dimensional vertical profiles of bulk electrical resistivity (ER) extracted from the 3D time-lapse images of the experimental waste rock pile (WRP). Black lines show ER vertical distribution before the infiltration event while blue and cyan lines show respectively ER distribution during and after infiltration. Dotted blue lines indicate GS3 sensor elevations (represented with black sensors).

1000 Ω m to 100 to 2000 Ω m. For instance, at $x = 15$ m, ER values in the ilmenite just below the FCL doubled, from 150 to 300 Ω m. Finally, the downslope part of the pile made of anorthosite waste rock (light-gray material in Fig. 6) showed a decrease of ER but remained fairly resistive after water infiltration (>20000 Ω m).

Three-Dimensional Inverted Changes in Bulk Electrical Resistivity during Infiltration

Figure 7 presents the temporal and spatial evolution of relative variations of bulk ER in the WRP before during and after the infiltration event. These images were obtained by calculating

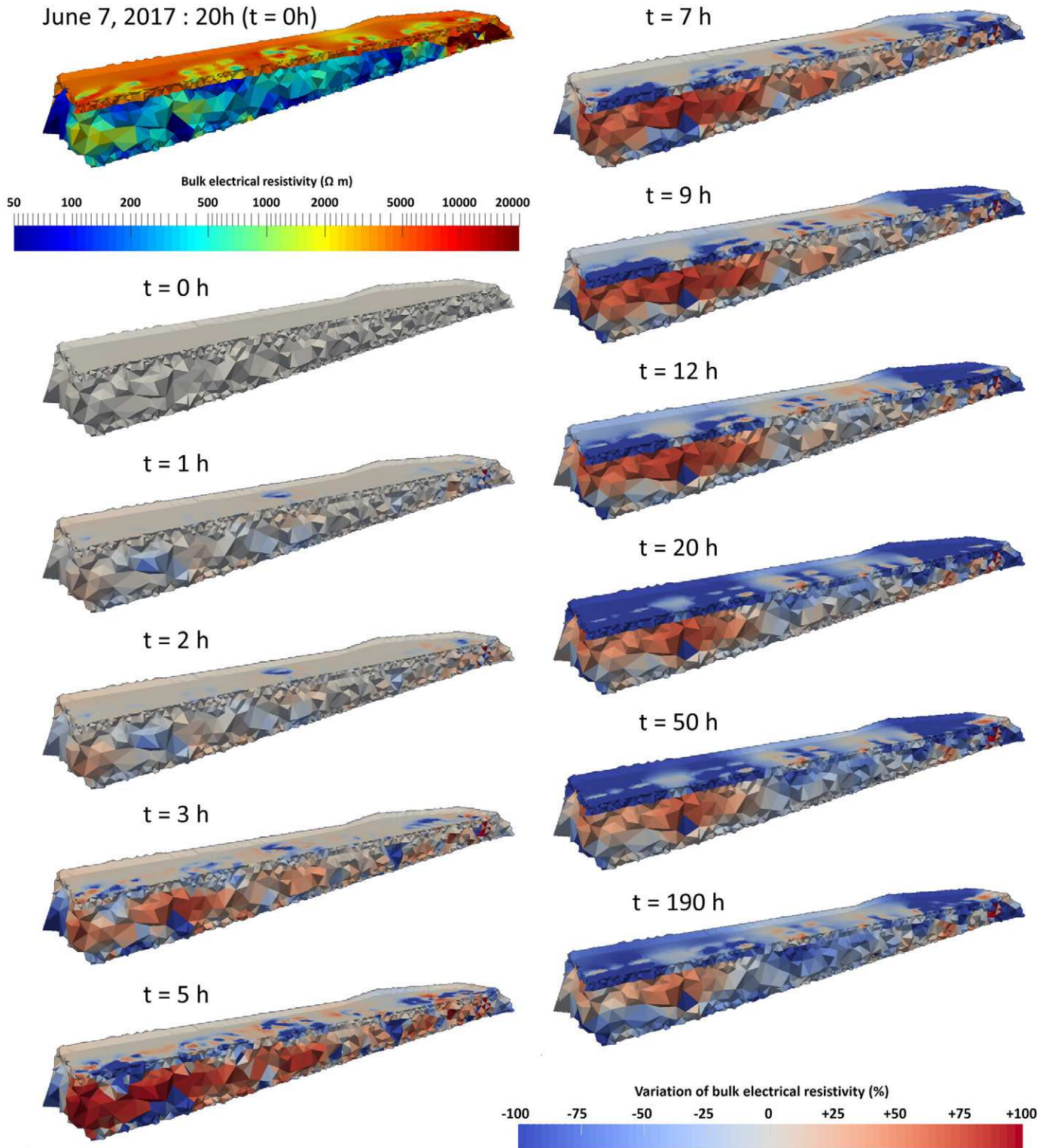


Fig. 7. Three-dimensional images of the inverted distribution of bulk electrical resistivity (ER) in the pile before the infiltration event (7 June at 20:00, $t = 0$ h, top left) and relative changes of ER during and after the water infiltration test. Red areas show where ER increased and the blue areas reflect a decrease as a result of water flow in the waste rock pile.

percentage changes (%) of the bulk ER values at different times (dates) relative to the starting image (7 June at 20:00). The top-left panel on Fig. 7 shows the distribution of inverted bulk ER in the pile before the infiltration event (cf. Fig. 5), which was used as the reference state. An increase of bulk ER compared with the starting image is denoted by a red color (and in blue for a decrease); areas where the ER remained constant over time are white. The data indicate that the FCL became less resistive after 5 h, especially near the downslope end of the pile where ER decreased by >75% after 9 h. The FCL was globally more conductive after 20 h from the start of the infiltration test, with variations ranging between 0 and -50% in the middle of the pile and between -75 and -100% near the upslope and downslope ends. In the same time, the bulk ER increased in the ilmenite waste rock by up to 75% (vs. initial ER value) 5 h after the beginning of the test. The ER values went back to their initial values 1 d after the infiltration test for the downslope part of the WRP in the ilmenite waste rocks. The highly resistive anorthosite zone near the end of the pile became globally more conductive after water infiltration, with relative variations ranging from -50 to -100%. However, some localized areas (elements) of the inverted model became more resistive in this zone (up to 100% of increase).

Evolution of Bulk and Water Electrical Resistivity Measured by GS3 Sensors

Evolution of Bulk Electrical Resistivity Measured by GS3 Sensors

Table 1 presents the evolution of bulk ER measured by GS3 sensors for two depths in the pile before and after the infiltration event (6 and 10 June) and the relative changes in percentage. The left panel presents GS3 measurements near the base of the compacted sand layer of the FCL (at a depth of 0.7 m from the surface), while the right panel presents GS3 measurements near the top of the coarse reactive ilmenite waste rock (just below the

Table 1. Evolution of the bulk electrical resistivity (ER) measured by GS3 sensors in the sand layer (flow control layer [FCL]) and near the top of the coarse reactive ilmenite waste rock (just below the interface with the FCL) before and after the infiltration event; the relative changes of bulk ER (%) are also given.

Lysimeter	GS3 position	Bulk ER in the sand measured with GS3 sensors			Bulk ER in the ilmenite measured with GS3 sensors		
		6 June	10 June	Change	6 June	10 June	Change
	m	— Ω m —	%		— Ω m —	%	
1	5	3500	1300	-63	10	12	20
2	15	1050	175	-83	26	32	23
3	25	1500	1200	-20	40	44	10
4†	35	1350	1350	0	575	1125	96
5	45	1600	450	-72	675	950	41
6	55	2250	250	-89	-	-	-
Mean value		1875	790	-58	265	435	64

† Bold text indicates the localization of the local concept model presented in Fig. 9 in the upper part of the waste rock pile at $x = 35$ m (Lysimeter 4).

interface with the FCL at a depth of 0.95 m). Bulk ER globally decreased in the sand layer during this period with mean value dropping from 1875 to 790 Ω m. The effect of the infiltration of conductive water ($\rho_w \approx 10$ Ω m, i.e., $EC \approx 1000$ μS cm⁻¹) in the FCL was particularly pronounced downslope of the pile, that is, for $50 \text{ m} < x < 60 \text{ m}$. At this location, bulk ER dropped from 2250 to 250 Ω m (a decrease of 89% from the initial ER value). In the meantime, GS3 sensors monitored a global increase of bulk ER below the FCL in the ilmenite waste rock. As indicated in the right panel of Table 1, the mean value increased from 265 to 435 Ω m (increase of 64%). The downslope part of the pile ($x > 30$ m) was somewhat more resistive than the upslope part; the increase of ER was also higher with values increasing from 600 to 1000 Ω m. The temporal evolution of bulk ER measured by GS3 sensors in the top part of the pile (at a depth <1.5 m) is presented in the left panel of Fig. A1 (Appendix for Lysimeter 4).

Influence of Water Quality Evolution on Bulk Electrical Resistivity

Figure 8 presents the temporal evolution of bulk ER and volumetric water content measured by a GS3 sensor located in the top sand layer (FCL) at $x = 35$ m (at a depth of 0.4 m). As indicated by the blue dotted line, the infiltration event had a strong effect on both bulk ER (blue line) and volumetric water content (red line). Bulk ER dropped from 2000 to ~250 Ω m and then remained constant during a week. In the meantime, the volumetric water content measured by the same GS3 probe increased from 0.08 to 0.16 after the infiltration event and returned to the initial value (0.08) after 2 d. These variations suggest that the nature of the water in the sand has been modified by the infiltration event. As the water sprinkled on the WRP was highly conductive ($\rho_w \approx 10$ Ω m, i.e., $EC \approx 1000$ μS cm⁻¹), the decrease of bulk ER could be associated with a decrease of water ER at this location in the top sand layer.

Evolution of Water Electrical Resistivity Measured with GS3 Sensors

The parameters obtained from the GS3 sensors measurements (bulk ER, volumetric water content, and temperature) were used to calculate the ER of water (ρ_w) in Ω m (or electrical conductivity EC in μS cm⁻¹). The theoretical background and the references used to perform this calculation are provided in the appendix. The temporal evolution of water ER measured by GS3 sensors in the top part of the pile (at a depth <1.5 m) is also presented on the right panel of Fig. A1 for Lysimeter 4 ($x = 35$ m). Table 2 presents the evolution of water ER measured by the GS3 sensors (presented above in Table 1) and the corresponding relative changes (%). All GS3 sensors in the sand layer (left panel of Table 2) monitored the same evolution of water ER. Water ER was fairly high before the infiltration event, with a mean value of 163 Ω m (corresponding to $EC = 61$ μS cm⁻¹), and then decreased after the infiltration event to a mean value of 41 Ω m ($EC = 244$ μS cm⁻¹). Water ER calculated for $x > 10$ m after the infiltration event is close to the ER of water that was sprinkled on top of the

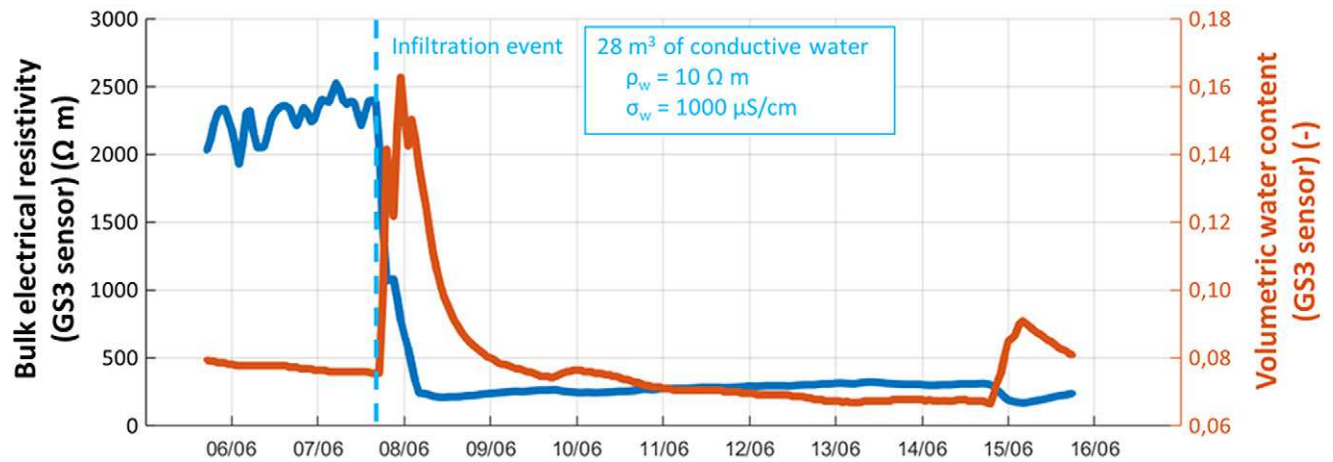


Fig. 8. Evolution of the bulk electrical resistivity (ER) and volumetric water content in the top sand layer (flow control layer) at $x = 35$ m ($z = 0.4$ m) as measured by a GS3 probe before, during, and after the infiltration event.

pile ($\rho_w \approx 10 \Omega \text{ m}$, i.e., $\text{EC} \approx 1000 \mu\text{S cm}^{-1}$). The data in the right panel of Table 2 indicate that the water contained in the ilmenite waste rock was more conductive in the upslope part of the pile ($x < 30$ m) vs. the downslope part. The mean value of water ER was $14 \Omega \text{ m}$ ($\text{EC} = 714 \mu\text{S cm}^{-1}$) for $x < 30$ m while it was $47 \Omega \text{ m}$ ($\text{EC} = 213 \mu\text{S cm}^{-1}$) for $x > 30$ m. The GS3 sensors monitored an increase of water ER in the ilmenite waste rock below the FCL with a mean ER value increasing from $27 \Omega \text{ m}$ ($\text{EC} = 370 \mu\text{S cm}^{-1}$) to $47 \Omega \text{ m}$ ($\text{EC} = 213 \mu\text{S cm}^{-1}$), an increase of 72%. This increase is particularly pronounced for the downslope part of the pile where water became more resistive (ρ_w ranging from 80 to 95 $\Omega \text{ m}$, i.e., EC between 105 and 125 $\mu\text{S cm}^{-1}$). The temporal evolution of water ER in the ilmenite waste rock below the FCL (at a depth of 0.95 m) is presented on the right panel of Fig. A1.

Analysis and Discussion

Applicability of Electrical Resistivity Tomography Monitoring for Water Infiltration in Mine Waste Rock Piles

The (quasi) static distribution of bulk ER in the experimental WRP obtained by ERT monitoring is consistent with the properties of the materials and geometry of the pile. The results presented above are in good agreement with previous studies on the electrical properties of ilmenite and anorthosite waste rocks for several mines in Québec (Anterrieu et al., 2010; Campos et al., 2003; Chouteau et al., 2010; Dimech et al., 2017; Poisson et al., 2009) and in the laboratory (Dawood et al., 2011; Dimech et al., 2018; Intissar, 2009). Anorthosite waste rocks are typically highly resistive (bulk ER $> 20000 \Omega \text{ m}$), while ilmenite waste rocks usually have a fairly low bulk ER (between 20 and $2000 \Omega \text{ m}$) because of their iron content.

Both spatial and temporal resolutions of ERT monitoring were increased in the WRP by using optimized protocols compared with the 2016 survey that used standard protocols (see Dimech et al. [2017] for more details concerning the sensitivity

and acquisition time of Wenner Schlumberger, gradient, and dipole–dipole protocols performed in 2016). Such optimized protocols can be used for any number of electrodes and any geometry to maximize the spatial resolution of ERT imagery while reducing the duration of data acquisition, hence increasing the temporal resolution as described by Wilkinson et al. (2010, 2012) and Loke et al. (2014a, 2014b). The quality of inversion results was enhanced here by using a high-resolution 3D model of the pile so geometry artifacts were largely avoided (Günther et al., 2006; Nimmer et al., 2008; Rücker et al., 2006); complex structural constraints were also successfully used (e.g., sharp variations between different layers and spatial smoothing in the same layer) (Johnson et al., 2010). The 3D distribution of electrode also proved to be efficient to monitor the entire WRP: measurements using electrodes near the top (or at the base) of the pile lead to a good spatial resolution at these locations, while measurements using simultaneously top

Table 2. Evolution of the water electrical resistivity (ER) calculated from GS3 sensor measurements in the sand layer (in the flow control layer [FCL]) and near the top of the coarse reactive ilmenite waste rocks (just below the interface with the FCL), before and after the infiltration event; the relative changes of water ER are also given.

Lysimeter	GS3 position	Water ER in the sand calculated from GS3 sensors			Water ER in the ilmenite calculated from GS3 sensors		
		6 June	10 June	Change	6 June	10 June	Change
	m	— $\Omega \text{ m}$ —		%	— $\Omega \text{ m}$ —		%
1	5	225	150	−33	6.5	8.5	31
2	15	110	20	−82	16	26	63
3	25	120	20	−83	19	25	32
4†	35	140	15	−89	45	95	110
5	45	180	25	−86	50	80	60
6	55	200	15	−93	–	–	–
Mean value		163	41	−75	27	47	72

† Bold text indicates the localization of the local concept model presented in Fig. 9 in the upper part of the waste rock pile at $x = 35$ m (Lysimeter 4).

and base electrodes provided good resolution in the core of the pile (as described by Kiflu et al. [2016] for a similar geometry).

The analysis and results presented in this study show that bulk ER was strongly affected by water infiltration in the experimental WRP. The FCL at the top of the pile became much more conductive after the infiltration event (average decrease of 60% of the bulk ER value). This decrease was observed by point-measurement sensors (GS3) and was also reconstructed by inversion from ERT monitoring datasets. However, the analysis of the volumetric water content and bulk ER showed that variations of the former were not the only cause of bulk ER variations. Temporal evolution of water ER was evaluated from GS3 measurements in the FCL, which indicated that water ER changed during water infiltration. This is consistent with the fact that water sprinkled on the top of the pile was highly conductive (water ER of $10 \Omega \text{ m}$, i.e., EC of $1000 \mu\text{S cm}^{-1}$), while the water present in the FCL before was more resistive (water ER ranging between 100 and $200 \Omega \text{ m}$, i.e., EC between 50 and $100 \mu\text{S cm}^{-1}$). The FCL water was originally associated with precipitation water that are usually fairly resistive. Water ER in the FCL dropped during the infiltration event by up to 93%. For this specific investigation, water ER variations was taken into account as fresh water infiltration both increased the volumetric water content and water EC in the FCL. A direct conversion of bulk ER into moisture content (assuming no changes of water ER) would have resulted in a great overestimation of the volumetric water content.

Both point-measurement sensors and ERT monitoring indicated that there was an increase of bulk ER in the conductive ilmenite waste rock in the core of the pile. This increase of bulk ER is greater in the downslope part of the WRP (up to 96% of the initial value) and less pronounced in the upslope part of the WRP (increase of 25%). This result may be somewhat counterintuitive as water infiltration is usually associated with a decrease of bulk ER (e.g., Binley et al., 2002; Singha et al., 2015). Also, a decrease of moisture content is not likely in the core of the pile after the infiltration event. Several studies have reported increasing values of bulk ER during water infiltration based on raw data (apparent resistivities) or from inverted results. The increase of bulk ER is usually considered as (i) an artifact created by the inversion process (e.g., Audebert et al., 2014; Clément et al., 2010; Descloitres et al., 2003, 2008; Hübner et al., 2015), (ii) the effect of a temperature decrease (e.g., Descloitres et al., 2003; Guérin et al., 2004), (iii) or of gas migration during water infiltration (e.g., Grellier et al., 2008; Uhlemann et al., 2016b), or (iv) of a change of water ER (e.g., Attia al Hagrey, 2007; Dumont et al., 2018; Hübner et al., 2015; Singha and Gorelick, 2005; Uhlemann et al., 2016b).

For the experimental WRP, local measurement in the conductive ilmenite waste rock by the GS3 sensors suggest that the increase of bulk ER may be an actual physical phenomenon rather than an inversion artifact. Moreover, it is highly improbable that the change of temperature ($<5^\circ\text{C}$) as a result of water infiltration can lead to an increase of 95% of the initial bulk ER value (Descloitres et al., 2003). The effect of water ER changes was thus investigated and was identified as the major contribution to bulk

ER variations during water infiltration. This is consistent with the GS3 sensors measurements, which lead to an average increase of 72% of water ER in the ilmenite waste rock below the FCL. The water in the upslope part of the WRP was highly conductive before water infiltration (water ER of $14 \Omega \text{ m}$, i.e., EC = $714 \mu\text{S cm}^{-1}$). This high conductivity was associated with high ionic concentrations (mainly calcium and sulfur, e.g., Martin et al., 2017; Plante et al., 2014; Poaty et al., 2018).

The increase of water ER during water infiltration may be interpreted as a transfer of resistive water from the FCL to the ilmenite waste rock underneath. The two types of water were thus mixed, resulting of a global increase of water ER and of bulk ER. The resistive water from the FCL may have replaced the conductive water in the downslope part of the ilmenite waste rock ($x > 30 \text{ m}$) where water ER almost reached a value of $100 \Omega \text{ m}$ (EC = $100 \mu\text{S cm}^{-1}$) at the end of the infiltration event. These results illustrate why water ER must be taken into account for this case, given that some waste rocks may ionize the pore water in the pile. This highly conductive water may then strongly affect bulk ER distribution during water infiltration and make it more difficult to interpret geoelectrical monitoring results (Robinson et al., 2008; Singha and Gorelick, 2005).

Electrical Resistivity Tomography Monitoring Provides Complementary Information to Describe Water Infiltration in the Waste Rock Piles

Three types of water were identified in the experimental WRP based on their water ER (i.e., ionic content) and the spatiotemporal evolution of bulk ER monitored in the WRP was used to track the flow of each type of water. Figure 9 introduces a conceptual model describing water infiltration in the upper part of the pile at $x = 35 \text{ m}$ (middle of the pile). This model is based on the temporal evolution of both bulk and water ER measured by GS3 sensors and reconstructed from geoelectrical monitoring of the pile. Water flow paths are shown at several dates in the crushed anorthosite waste rocks (gray), in the compacted sand (yellow), and in the coarse ilmenite waste rocks (brown). Three types of water are shown: resistive water in red (ER $\approx 100 \Omega \text{ m}$ or EC $\approx 100 \mu\text{S cm}^{-1}$), conductive water in blue (ER $\approx 10 \Omega \text{ m}$ or EC $\approx 1000 \mu\text{S cm}^{-1}$), and water with an intermediate resistivity value in orange (ER $\approx 50 \Omega \text{ m}$ or EC $\approx 200 \mu\text{S cm}^{-1}$). The resistive water associated with previous precipitations was present in the FCL (sand) before the artificial infiltration event (line with bold text Table 2). The water ER of intermediate water located in the ilmenite waste rock was attributed to a high ionic concentration (mostly calcium and sulfur ions, as identified by Plante et al. [2014]). The conductive water was used to simulate a large precipitation event in the WRP with a water truck. The large contrast of water ER in the WRP before infiltration allowed to track each type of water with ERT monitoring and point measurements. As a result, infiltration of fresh conductive water was imaged as a drop of bulk and water ER in the FCL, while percolation of old resistive water from the FCL to the ilmenite waste rocks was tracked from water and bulk ER increase in the core of the WRP.

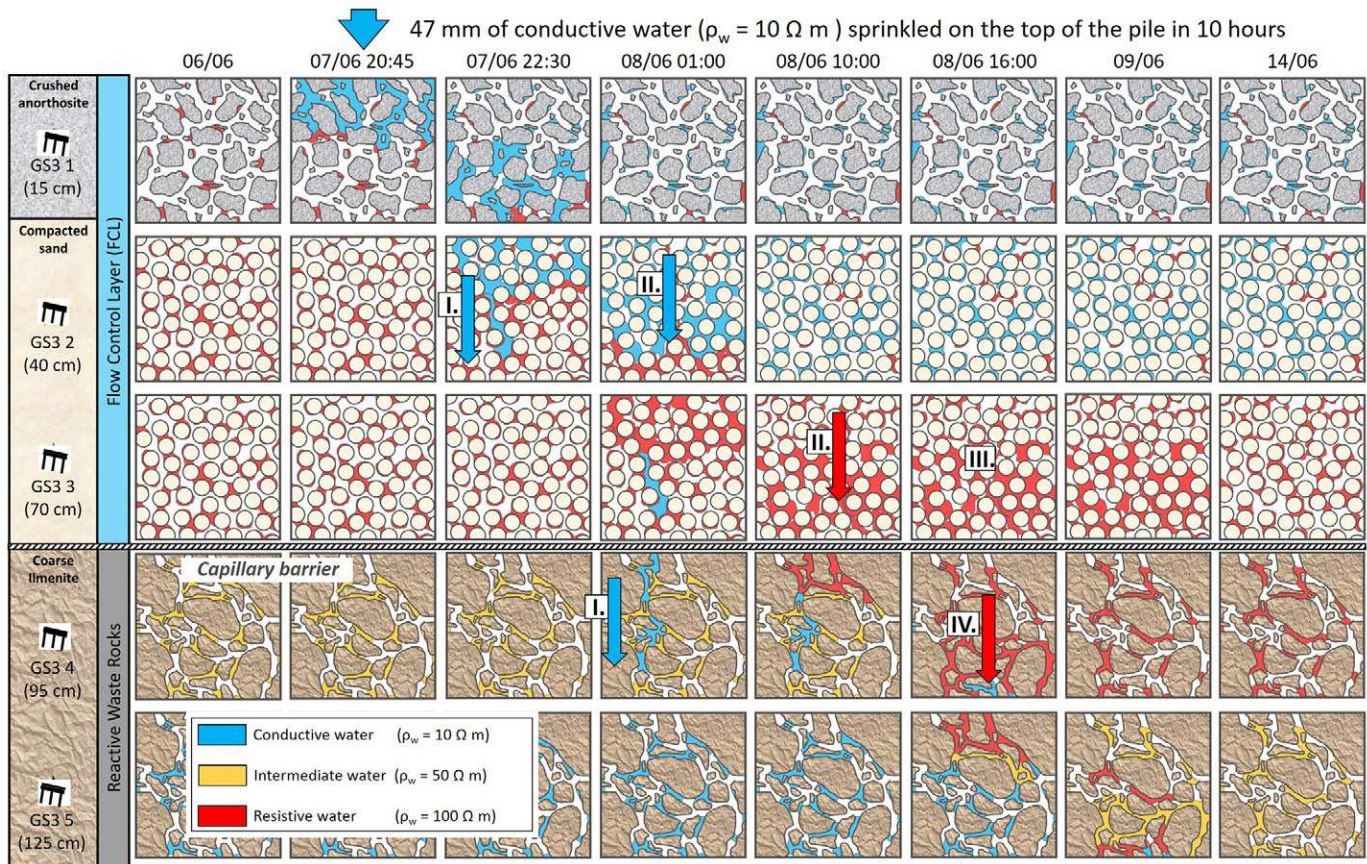


Fig. 9. Conceptual model of water infiltration in the upper part of the WRP at $x = 35 \text{ m}$. Red water corresponds to water ER of $100 \Omega \text{ m}$ ($100 \mu\text{S}/\text{cm}$); orange: $50 \Omega \text{ m}$ ($200 \mu\text{S}/\text{cm}$); blue: $10 \Omega \text{ m}$ ($1000 \mu\text{S}/\text{cm}$). Types of flows: I, fast vertical flow in macropores; II, slower vertical flow in the sand matrix; III, water accumulation at the bottom of the flow control layer (FCL); IV, the percolation of water through the FCL in the waste rocks.

Figure 9 presents three infiltration modes identified by using water ER as a tracer. A fast vertical flow in macropores (Fig. 9I) occurred in the waste rocks, as described by Peregoedova et al. (2013) and Broda et al. (2013a). This fast flow would explain the quick decrease of water ER monitored by some of the GS3 sensors in the ilmenite waste rocks after the infiltration event (Appendix). A slower vertical flow was observed in the sand matrix of the FCL (Fig. 9II). During this conventional unsaturated subsurface flow, the fresh conductive water (blue) replaced the old resistive water (red) in the pores of the sand. This water displacement phenomenon was also discussed in several hydrogeophysical studies using natural or artificial tracers (e.g., Garré et al., 2010; Koestel et al., 2008; Scaini et al., 2017; Singha and Gorelick, 2005). The increase of water ER over time in the bottom of the FCL (Fig. 9III) was interpreted as a capillary barrier effect (deemed to occur at the base of the inclined FCL; e.g., Aubertin et al., 2009). Resistive water coming from the sand upslope was diverted laterally toward the end of the pile. Part of this resistive water percolated in the reactive waste rocks, where it replaced the conductive water (Fig. 9IV), resulting in the increase of bulk and water ER as previously stated. This conceptual model is consistent with water and bulk ER spatiotemporal variations observed by both point-measurement sensors and ERT monitoring. Several studies also used ERT monitoring of tracer infiltration to

propose conceptual models describing the observed hydrogeological processes (e.g., Hübner et al., 2017; Scaini et al., 2017; Slater et al., 2000). However, this conceptual model remains qualitative and could be refined by using a smaller electrode spacing to increase spatial resolution of ERT monitoring following the example of Hübner et al. (2017). Also, it would be interesting to use to use borehole electrodes with a small vertical spacing as presented in (Kuras et al., 2009) to increase vertical resolution in the FCL. The local conceptual model presented on Fig. 9 was extended to propose a global model describing water infiltration water for the entire experimental WRP. The global model shown by Fig. 10 relies on the spatiotemporal evolution of bulk and water ER monitored by point-measurement sensors and ERT monitoring $\sim 24 \text{ h}$ after the infiltration event. The color code used for the materials of the pile is described in Fig. 9 and the same types of water are used to describe water infiltration.

The increase of water ER monitored by point-measurement sensors in the ilmenite waste rock was used as a proxy to evaluate how much resistive water percolated from the FCL into the ilmenite waste rock (Fig. 9IV flow), hence replacing ionized conductive water. As a result, more resistive water seemed to infiltrate into the ilmenite waste rocks for the downslope part of the pile in comparison with the upslope part. This result illustrated by larger red arrows on Fig. 10 suggested that a capillary barrier effect occurred in the upslope

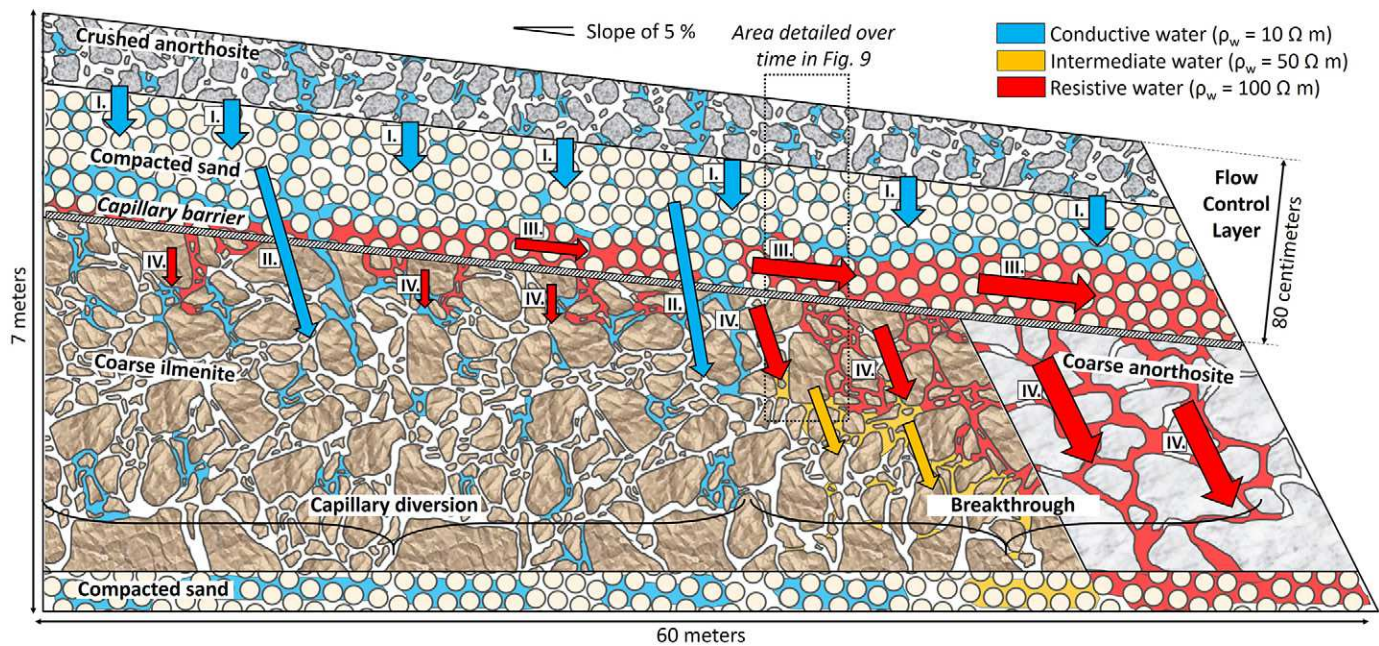


Fig. 10. Global conceptual model of water infiltration in the experimental waste rock pile. Three types of water with specific electrical resistivity (ER) values are identified (blue, orange and red). After the infiltration event, fresh conductive water (in blue) replaced old resistive water (in red) in the flow control layer. This resistive water was diverted laterally by the capillary barrier effect and percolated downslope, predominantly in the nonreactive coarse anorthosite waste rocks where a breakthrough occurred. Types of flows: I, fast vertical flow in macropores; II, slower vertical flow in the sand matrix; III, water accumulation at the bottom of the flow control layer (FCL); IV, the percolation of water through the FCL in the waste rocks.

part of the WRP (indicated as capillary diversion zone) while a breakthrough was deemed to occur in the downslope part of the WRP. A lateral deviation of resistive water in the upslope part of the FCL (Fig 10III) was supposed to occur, thus increasing water content in the downslope part of the FCL as illustrated by large semihorizontal arrows on Fig. 10. This capillary effect seemed to be consistent with previous hydrogeological studies. Fala et al. (2005, 2006) and (Aubertin et al., 2009) showed that lateral deviation of infiltration water can occur when the contrast of a fine layer and a coarse material creates a capillary barrier effect with numerical simulations. Hydrogeological modeling was used to evaluate the efficiency of a FCL made of compacted sand for different lengths and slope angles on WRP. Broda et al. (2017) also used numerical simulations to evaluate the influence of fractures and macropores on the efficiency of the FCL. They showed that fractures can limit the capillary barrier effect and increase the infiltration of water in the reactive waste rocks. Finally, the lateral diversion of water created by a capillary barrier effect at a field-scale site was also observed with hydrogeophysical monitoring (Hübner et al., 2017).

The simplified model describing water infiltration in the WRP was supported by all point-measurement sensors (both water and bulk ER values). In addition, preliminary results from the geochemical analyses indicated that the water ER of the leachates at the base of the pile was consistent with the proposed model (see Poaty et al. [2018] for more information). Finally, the lysimeters at the base of the WRP allowed evaluation of cumulated volumes of water percolating into the waste rocks. It seemed that more water was collected on the downslope part of the pile, which would be in

agreement with the proposed model (Dubuc et al., 2017). Further work is underway to evaluate the efficiency of the FCL with all the monitoring techniques used on the experimental WRP of the Lac Tio mine. These results might help to evaluate the FCL efficiency for extreme precipitations and would be used to describe the hydrogeological behavior of WRPs. Also, the results can be used to refine numerical models and simulate water infiltration for diverse geometries of FCL and future climate conditions.

Conclusion

The hydrogeological behavior of mine WRP is difficult to assess because of the nature of the materials and inherent heterogeneity in these large structures. A controlled precipitation test (simulating a large precipitation event) was performed and monitored by several techniques to evaluate water flow in a WRP covered by a FCL made of compacted sand. This study evaluates the applicability of hydrogeophysical monitoring in the context of a mine WRP with time-lapse electrical tomography to complement traditional point measurements. Bulk ER variations were strongly affected by both water nature and water flows in the WRP and geoelectrical results were consistent with point measurements. Water ER was used as tracers to track the infiltration paths of several types of water in the experimental WRP. Conceptual models were proposed to describe hydrogeological processes observed in the WRP. The local and global model describing water flows in the pile were used to complement moisture sensors. A capillary barrier effect was observed in the upslope part of the pile while a

breakthrough occurred in the downslope part of the pile during the infiltration event. These results will be compared with other monitoring techniques (such as distributed temperature sensors and flow meters at the base of the pile) and will help to refine numerical simulations of WRPs to evaluate and optimize the long-term efficiency of future reclamation techniques.

Appendix

Calculation of Water Electrical Resistivity from GS3 Sensor Measurements

Determination of water electrical resistivity (ER) calculated from the GS3 sensors can help refine the hydrogeological interpretation of bulk ER images by separating the effect of moisture

content from that of water ER. A relationship can be established to estimate the water ER from the bulk ER of the medium, the volumetric water content, and the temperature measured by the GS3 sensors based on the work of (Hilhorst, 2000). Water ER ρ_w can be determined from the following equation (Decagon Devices, 2016):

$$\rho_w = \frac{(\epsilon_b - \epsilon_{\rho_b=\infty})\rho_b}{\epsilon_w} \quad [A1]$$

where ρ_b is the medium ER (Ω m), ϵ_b and ϵ_w are respectively the real part of the dielectric constant of the medium and the water (unitless), and $\epsilon_{\rho_b=\infty}$ is the real part of the dielectric constant for a dry medium (unitless). The value of $\epsilon_{\rho_b=\infty}$ equals 4.1 to ensure consistency with the GS3 probes calibration (Hilhorst, 2000).

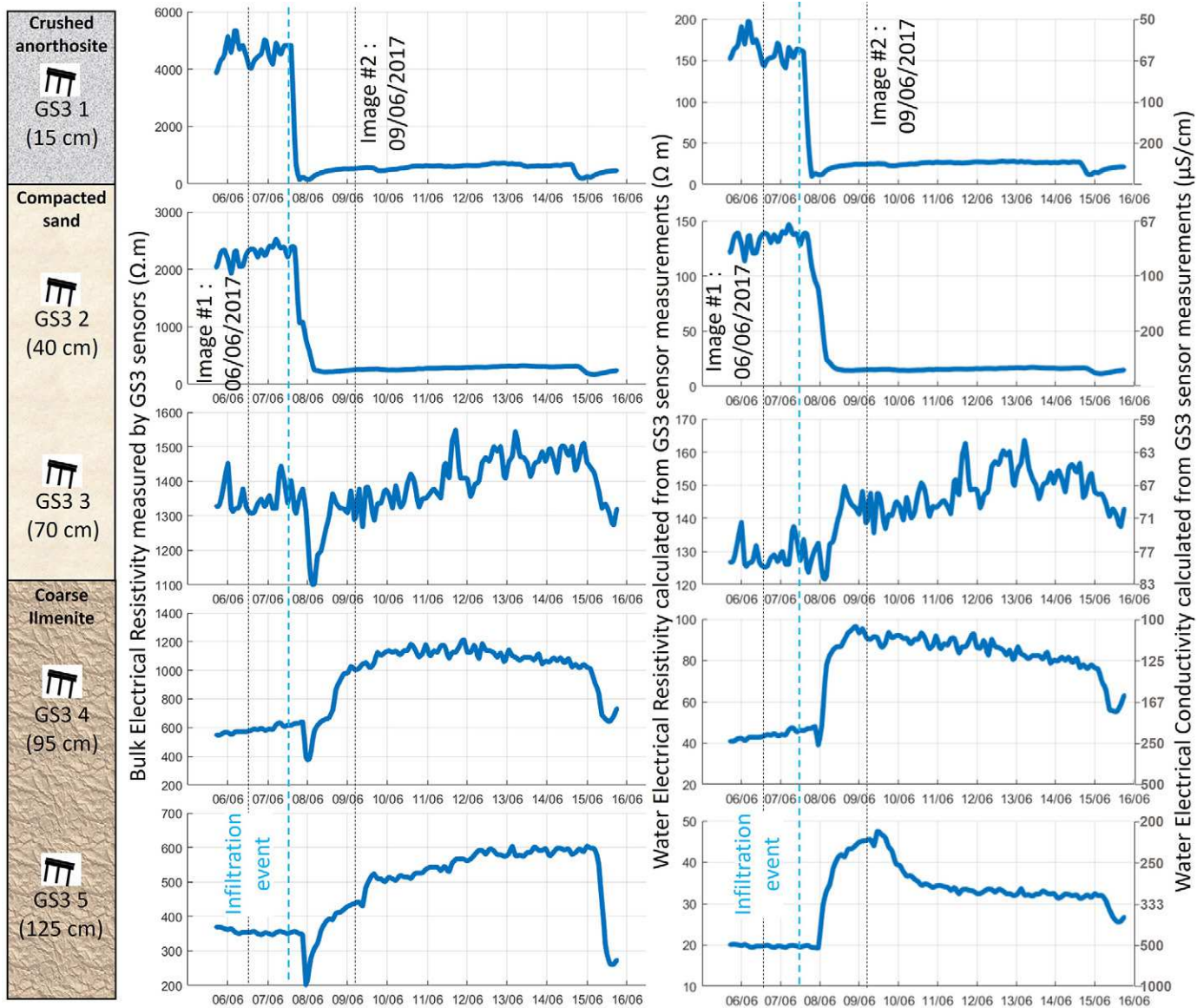


Fig. A1. Variation of the bulk electrical resistivity (ER) and water ER near the top of the pile measured by GS3 probes at $x = 35$ m. Water ERs were calculated from point sensor measurements (moisture content, bulk ER, and temperature). Black dotted lines correspond to the dates of the images shown in Fig. 5, while blue dotted lines indicate the date of the infiltration event. The diagram on the left displays sensor locations and the type of medium in a vertical cross-section of the pile.

An empirical relation links ϵ_w and T_{med} , the temperature of the medium measured by the GS3 sensor (Decagon Devices, 2016):

$$\epsilon_w = 80.3 - 0.37(T_{med} - 20) \quad [A2]$$

The calibration equation used by GS3 sensors to compute the volumetric water content (VWC) can be expressed as follows (Decagon, 2016):

$$VCW = 0.118\sqrt{\epsilon_b} - 0.117 \quad [A3]$$

The combination of Eq. [A1], [A2], and [A3] gives the following relationship to calculate ρ_w from the parameters measured by GS3 sensor (ρ_b , T_{med} , and VWC) (Decagon, 2016):

$$\rho_w = \frac{[(VWC + 0.117)/0.118]^2 - 4.1}{80.3 - 0.37(T_{med} - 20)} \rho_b \quad [A4]$$

Equation [A4] was used to calculate the evolution of water ER at each GS3 sensor location. The evolution of water ER over time is presented in Fig. A1 for GS3 sensors located near the top of the

pile (in the FCL and in ilmenite waste rocks) at $x = 35$ m. Bulk ER are also represented before, during, and after the infiltration event (using dotted blue lines). This figure points out the complex temporal variations of both bulk and water ER in the waste rock pile as a result of water infiltration. The diagram on the left of Fig. A1 details the position of each GS3 sensor and specifies the nature of the materials (crushed anorthosite waste rocks and sand for the FCL and coarse ilmenite waste rocks). The GS3 sensors in the FCL measured a drop of bulk ER immediately after the infiltration event (from 2000–5000 to 250 Ω m) while GS3 sensors in the reactive waste rocks measured a quick drop followed by an increase of ER (from 600 to 1200 Ω m at $z = 0.95$ m).

The increase of water ER measured near the top of the ilmenite waste rocks with GS3 sensor presented in Fig. A1 ($x = 35$ m, $z = 0.95$ m) was not measured all along the pile as shown in Table 2. Water ER calculated from GS3 sensors measurements for $x < 30$ m remained low ($\rho_w \approx 5\text{--}25 \Omega$ m or $400\text{--}2000 \mu\text{S cm}^{-1}$) after the infiltration event. The increase of water ER was only measured for $x > 30$ m where water ER doubled from 50 to 100 Ω m (corresponding to a decrease of EC from 200 to 100 $\mu\text{S cm}^{-1}$). Figure

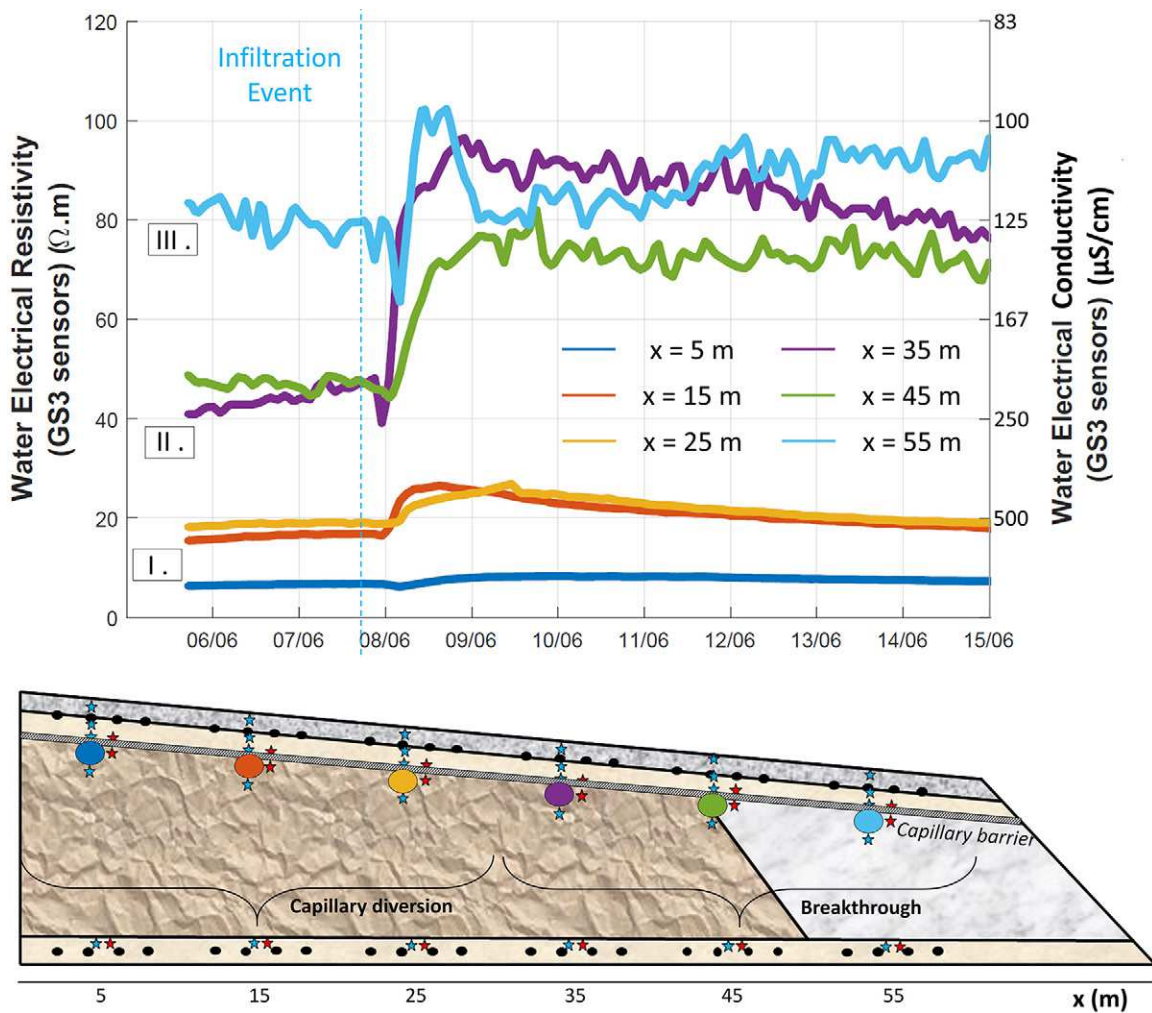


Fig. A2. Variation of water electrical resistivity (ER) over time after the infiltration event for several positions in the coarse waste rocks. Water ER increased drastically downslope after infiltration (as a result of some percolation). Positions of GS3 probes are presented with colored dots on a 2D section of the pile.

A2 summarizes the temporal evolution of water ER calculated from GS3 measurements according to Eq. [A4]. A 2D longitudinal section of the pile indicates the location of GS3 sensors just below the capillary barrier; the date of water infiltration event is marked by a blue dotted line. Three modes of water ER variations are referred to in Fig. A2 as (I), (II), and (III). As summarized in Table 2, pore water near the top of the ilmenite waste rocks was highly conductive for $x < 30$ m (Fig. A2I). The infiltration event had a negligible effect on water ER for $x < 30$ m. Evolution of water ER was similar for $x = 15$ m and $x = 25$ m: water ER increased from 20 to 30 Ω m (decrease of EC from 500 to 333 $\mu\text{S cm}^{-1}$) after the infiltration event, and returned to initial values after about a week. The water contained in the ilmenite waste rocks around the GS3 sensors located at $x = 35$ m and $x = 45$ m was slightly more resistive before water infiltration (Fig. A2II). The infiltration event had a strong effect on the quality of water at these locations, as shown in Fig. A2: water ER increased from 40 to 90 Ω m (EC decreased from 250 to 111 $\mu\text{S cm}^{-1}$) after the infiltration event and remained around 80 Ω m (EC \approx 125 $\mu\text{S cm}^{-1}$) during a week. This evolution suggested that the water with intermediate resistivity was replaced by more resistive water, which would also indicate that some water infiltration occurred in the waste rocks for $x > 30$ m (across the interface with the capillary barrier). Finally, the GS3 sensor located near the top of the anorthosite waste rocks monitored a slight increase of water ER (Fig. A2III).

Acknowledgments

We would like to acknowledge the financial support from NSERC and the industrial partners of the Research Institute on Mines and the Environment (<http://irme.ca/>). Also, this project would not have been possible without support of the employees of the Lac Tio mine and the effort of the technicians, students, and interns who contributed to the construction and monitoring of the waste rock pile. We also thank two anonymous reviewers for their helpful comments on our original manuscript.

References

- ABEM Instrument. 2016. Terrameter LS instruction manual. ABEM Instrument, Sundbyberg, Sweden.
- Amos, R.T., D.W. Blowes, B.L. Bailey, D.C. Segó, L. Smith, and A.I.M. Ritchie. 2015. Waste-rock hydrogeology and geochemistry. *Appl. Geochem.* 57:140–156. doi:10.1016/j.apgeochem.2014.06.020
- Anterrieu, O., M. Chouteau, and M. Aubertin. 2010. Geophysical characterization of the large-scale internal structure of a waste rock pile from a hard rock mine. *Bull. Eng. Geol. Environ.* 69:533–548. doi:10.1007/s10064-010-0264-4
- Archie, G.E. 1942. The electrical resistivity log as an aid in determining some reservoir characteristics. *Trans. AIME* 146:54–62. doi:10.2118/942054-G
- Attia, A.M., D. Fratta, and Z. Bassiouni. 2008. Irreducible water saturation from capillary pressure and electrical resistivity measurements. *Oil Gas Sci. Technol.* 63:203–217.
- Attia al Hagrey, S. 2007. Geophysical imaging of root-zone, trunk, and moisture heterogeneity. *J. Exp. Bot.* 58:839–854. doi:10.1093/jxb/erl237
- Aubertin, M. 2013. Waste rock disposal to improve the geotechnical and geochemical stability of piles. Paper presented at the 23rd World Mining Congress, Montréal. 11–15 Aug. 2013. *Can. Inst. Min. Metall. Pet., Westmount, QC.*
- Aubertin, M., E. Cifuentes, S. Apithy, B. Bussière, J. Molson, and R. Chapuis. 2009. Analyses of water diversion along inclined covers with capillary barrier effects. *Can. Geotech. J.* 46:1146–1164. doi:10.1139/T09-050
- Audebert, M., R. Clément, J. Grossin-Debattista, T. Günther, N. Touze-Foltz, and S. Moreau. 2014. Influence of the geomembrane on time-lapse ERT measurements for leachate injection monitoring. *Waste Manage.* 34:780–790. doi:10.1016/j.wasman.2014.01.011
- Audebert, M., R. Clément, S. Moreau, C. Duquennoi, S. Loisel, and N. Touze-Foltz. 2016a. Understanding leachate flow in municipal solid waste landfills by combining time-lapse ERT and subsurface flow modelling: I. Analysis of infiltration shape on two different waste deposit cells. *Waste Manage.* 55:165–175. doi:10.1016/j.wasman.2016.04.006
- Aubertin, M., O. Fala, B. Bussière, V. Martin, D. Campos, A. Gamache-Rochette, et al. 2002. Analyse des écoulements de l'eau en conditions non saturées dans les haldes à stériles. In: *Proceedings of the symposium sur l'environnement et les mines: Défis et perspectives*, Rouyn-Noranda, QC, Canada. 3–5 Nov. 2002. *Can. Inst. Min. Metall. Pet., Westmount, QC.*
- Aubertin, M., O. Fala, J. Molson, M. Chouteau, O. Anterrieu, M.A. Hernandez, et al. 2008. Caractérisation du comportement hydrogéologique et géochimique des haldes à stériles. In: *Proceedings of the symposium sur l'environnement et les mines*, Rouyn-Noranda, QC, Canada. 2–5 Nov. 2008. *Can. Inst. Min. Metall. Pet., Westmount, QC.*
- Aubertin, M., O. Fala, J. Molson, A. Gamache-Rochette, B. Lahmira, V. Martin, et al. 2005. Évaluation du comportement hydrogéologique et géochimique des haldes à stériles. In: *Proceedings of the Symposium sur l'environnement et les mines*, Rouyn-Noranda, QC, Canada. 15–18 May 2005. *Can. Inst. Min. Metall. Pet., Westmount, QC.*
- Audebert, M., L. Oxarango, C. Duquennoi, N. Touze-Foltz, N. Forquet, and R. Clément. 2016b. Understanding leachate flow in municipal solid waste landfills by combining time-lapse ERT and subsurface flow modelling—Part II: Constraint methodology of hydrodynamic models. *Waste Manage.* 55:176–190. doi:10.1016/j.wasman.2016.04.005
- Bechtold, M., J. Vanderborght, L. Weiermüller, M. Herbst, T. Günther, O. Ippisch, et al. 2012. Upward transport in a three-dimensional heterogeneous laboratory soil under evaporation conditions. *Vadose Zone J.* 11(2). doi:10.2136/vzj2011.0066
- Binley, A., G. Cassiani, R. Deiana. 2010. Hydrogeophysics: Opportunities and challenges. *Boll. Geofis. Teor. Ed. Appl.* 51:267–284.
- Binley, A., S.S. Hubbard, J.A. Huisman, A. Revil, D.A. Robinson, K. Singha, and L.D. Slater. 2015. The emergence of hydrogeophysics for improved understanding of subsurface processes over multiple scales. *Water Resour. Res.* 51:3837–3866. doi:10.1002/2015WR017016
- Binley, A., B. Shaw, and S. Henry-Poulter. 1996. Flow pathways in porous media: Electrical resistance tomography and dye staining image verification. *Meas. Sci. Technol.* 7:384. doi:10.1088/0957-0233/7/3/020
- Binley, A., P. Winship, L.J. West, M. Pokar, and R. Middleton. 2002. Seasonal variation of moisture content in unsaturated sandstone inferred from borehole radar and resistivity profiles. *J. Hydrol.* 267:160–172. doi:10.1016/S0022-1694(02)00147-6
- Blackmore, S., D. Pedretti, K. Mayer, L. Smith, and R. Beckie. 2018. Evaluation of single- and dual-porosity models for reproducing the release of external and internal tracers from heterogeneous waste-rock piles. *J. Contam. Hydrol.* 214:65–74. doi:10.1016/j.jconhyd.2018.05.007
- Bréard Lanoix, M.L. 2017. Caractérisation des propriétés hydrogéologiques de la couche de contrôle des écoulements placée sur la halde à stériles expérimentale à la mine du lac Tio. École Polytechnique de Montréal.
- Broda, S., M. Aubertin, D. Blessent, E. Hirthe, and T. Graf. 2017. Improving control of contamination from waste rock piles. *Environ. Geotech.* 4:274–283. doi:10.1680/envgeo.14.00023
- Broda, S., E. Hirthe, D. Blessent, M. Aubertin, and T. Graf. 2013a. Using random discrete fractures for representing preferential flow in waste rock piles with compacted layers. Paper presented at the 66th Canadian Geotechnical Conference, Montréal, QC, Canada. 29 Sept.–3 Oct. 2013. *Can. Geotech. Soc., Richmond, BC.*
- Broda, S., C. Sayde, J. Selker, M. Aubertin, and D. Blessent. 2013b. Using temperature as a tracer for analyzing the response of a capillary barrier in waste rock. Paper presented at the 66th Canadian Geotechnical

- Conference, Montréal, QC, Canada. 29 Sept.–3 Oct. 2013. Can. Geotech. Soc., Richmond, BC.
- Bussière, B., M. Aubertin, G.J. Zagury, R. Potvin, and M. Benzaazoua. 2005. Principaux défis et pistes de solution pour la restauration des aires d'entreposage de rejets miniers abandonnées. In: Proceedings of the Symposium sur l'environnement et les mines, Rouyn-Noranda, QC, Canada. 15–18 May 2005. Can. Inst. Min., Metall. Pet., Westmount, QC.
- Bussière, B., B. Plante, S. Broda, M. Aubertin, D. Chen, and F. Medina. 2015. Contrôle des infiltrations d'eau dans les haldes à stériles à l'aide des effets de barrière capillaire: Design, construction et instrumentation de la halde expérimentale de la mine Tio. In: Proceedings of the Symposium sur l'environnement et les mines, Rouyn-Noranda, QC, Canada. 14–17 June 2015. Can. Inst. Min., Metall. Pet., Westmount, QC.
- Campos, D., M. Chouteau, M. Aubertin, and B. Bussière. 2003. Using geophysical methods to image the internal structure of mine waste rock piles. In: Proceedings of the European Meeting of Environmental and Engineering Geophysics, Prague, Czech Republic. 31 Aug.–4 Sept. 2003. doi:10.3997/2214-4609.201414485
- Cassiani, G., N. Ursino, R. Deiana, G. Vignoli, J. Boaga, M. Rossi, et al. 2012. Noninvasive monitoring of soil static characteristics and dynamic states: A case study highlighting vegetation effects on agricultural land. *Vadose Zone J.* 11(3). doi:10.2136/vzj2011.0195
- Chambers, J., D. Gunn, P. Wilkinson, P. Meldrum, E. Haslam, S. Holyoake, et al. 2014. 4D electrical resistivity tomography monitoring of soil moisture dynamics in an operational railway embankment. *Near Surf. Geophys.* 12:61–72. doi:10.3997/1873-0604.2013002
- Chambers, J.E., P.I. Meldrum, P.B. Wilkinson, W. Ward, C. Jackson, B. Matthews, et al. 2015. Spatial monitoring of groundwater drawdown and rebound associated with quarry dewatering using automated time-lapse electrical resistivity tomography and distribution guided clustering. *Eng. Geol.* 193:412–420. doi:10.1016/j.enggeo.2015.05.015
- Chou, T.K., M. Chouteau, and J.S. Dubé. 2016. Estimation of saturated hydraulic conductivity during infiltration test with the aid of ERT and level-set method. *Vadose Zone J.* 15(7). doi:10.2136/vzj2015.05.0082
- Chouteau, M., R. Intissar, and M. Aubertin. 2010. Internal structure of an ilmenite mine waste rock pile modelled from IP imaging and laboratory measurements. In: Proceedings of the 23rd EEGS Symposium on the Application of Geophysics to Engineering and Environmental Problems, Nashville, TN. 25–29 Mar. 2010. Soc. Explor. Geophys., Tulsa, OK. doi:10.4133/1.3445462
- Clément, R., M. Descloitres, T. Günther, L. Oxarango, C. Morra, J.P. Laurent, and J.P. Gourc. 2010. Improvement of electrical resistivity tomography for leachate injection monitoring. *Waste Manage.* 30:452–464. doi:10.1016/j.wasman.2009.10.002
- Clément, R., S. Moreau, H. Henine, A. Guérin, C. Chaumont, and J. Tournebize. 2014. On the value of combining surface and cross-borehole ERT measurements to study artificial tile drainage processes. *Near Surf. Geophys.* 12:763–775. doi:10.3997/1873-0604.2014034
- Dawood, I., M. Aubertin, R. Intissar, and M. Chouteau. 2011. A combined hydrogeological–geophysical approach to evaluate unsaturated flow in a large waste rock pile. In: Proceedings of the 14th Pan-American Conference on Soil Mechanics and Geotechnical Engineering, Toronto, ON, Canada. 2–6 Oct. 2011. Int. Soc. Soil Mech. Geotech. Eng., London.
- Decagon Devices. 2016. GS3 water content, EC temperature sensor: Operator's manual. Decagon Devices, Pullman, WA.
- Decagon Devices. 2017. MPS-2 and MPS-6 dielectric water potential sensors operator's manual. Decagon Devices, Pullman, WA.
- Descloitres, M., O. Ribolzi, and Y. Le Troquer. 2003. Study of infiltration in a Sahelian gully erosion area using time-lapse resistivity mapping. *Catena* 53:229–253. doi:10.1016/S0341-8162(03)00038-9
- Descloitres, M., L. Ruiz, M. Sekhar, A. Legchenko, J. Braun, M. Mohan Kumar, and S. Subramanian. 2008. Characterization of seasonal local recharge using electrical resistivity tomography and magnetic resonance sounding. *Hydrol. Processes* 22:384–394. doi:10.1002/hyp.6608
- Dimech, A. 2018. Imagerie de l'écoulement de l'eau dans une halde à stériles expérimentale par tomographie 3D de résistivité électrique. M.S. thesis. École Polytechnique de Montréal.
- Dimech, A., M. Chouteau, B. Bussière, V. Martin, M. Aubertin, and B. Plante. 2018. 3D time-lapse geoelectrical monitoring of moisture content in an experimental waste rock pile: Validation using hydrogeological data. In: Symposium on the Application of Geophysics to Engineering and Environmental Problems, Nashville, TN. 25–29 Mar. 2018. Soc. Explor. Geophys., Tulsa, OK. p. 92–99. doi:10.4133/sageep.31-009
- Dimech, A., M. Chouteau, É. Chou, M. Aubertin, V. Martin, B. Bussière, and B. Plante. 2017. Monitoring water infiltration in an experimental waste rock pile with time-lapse ERT and multi-parameter data collection. In: Proceedings of the Symposium on the Application of Geophysics to Engineering and Environmental Problems, Denver, CO. 19–23 Mar. 2017. Soc. Explor. Geophys., Tulsa, OK. doi:10.4133/SAGEEP.30-009
- Dubuc, J., 2018. Étude du comportement hydrogéologique d'une couche de contrôle des écoulements placée à la surface d'une halde à stériles expérimentale. M.S. thesis. Univ. of Montreal.
- Dubuc, J., T. Pabst, and M. Aubertin. 2017. An assessment of the hydrogeological response of the flow control layer installed on the experimental waste rock pile at the Lac Tio mine. In: Proceedings of the 70th Canadian Geotechnical Society Conference: 70 Years of Canadian Geotechnics and Geoscience, GeoOttawa 2017, Ottawa, ON. 1–4 Oct. 2017. Can. Geotech. Soc., Richmond, BC.
- Dumont, G., T. Pilawski, T. Hermans, F. Nguyen, and S. Garré. 2018. The effect of initial water distribution and spatial resolution on the interpretation of ERT monitoring of water infiltration in a landfill cover. *Hydrol. Earth Syst. Sci. Discuss.* doi:10.5194/hess-2018-163
- Fala, O., M. Aubertin, J. Molson, B. Bussière, G. Wilson, R. Chapuis, and V. Martin. 2003. Numerical modelling of unsaturated flow in uniform and heterogeneous waste rock piles. In: Proceedings of the Sixth International Conference on Acid Rock Drainage, Cairns, Queensland. 14–17 July 2003. Australasian Inst. Min. Metall., Carlton, VIC, Australia. p. 895–902.
- Fala, O., J. Molson, M. Aubertin, and B. Bussière. 2005. Numerical modelling of flow and capillary barrier effects in unsaturated waste rock piles. *Mine Water Environ.* 24:172–185. doi:10.1007/s10230-005-0093-z
- Fala, O., J. Molson, M. Aubertin, B. Bussière, and R.P. Chapuis. 2006. Numerical simulations of long term unsaturated flow and acid mine drainage at waste rock piles. In: Proceedings of the 7th International Conference on Acid Rock Drainage and SME Annual Meeting, St. Louis, MO. 26–30 Mar. 2006. Am. Soc. Min. Reclam., Champaign, IL. p. 26–30.
- Garré, S., J. Koestel, T. Günther, M. Javaux, J. Vanderborght, and H. Vereecken. 2010. Comparison of heterogeneous transport processes observed with electrical resistivity tomography in two soils. *Vadose Zone J.* 9:336–349. doi:10.2136/vzj2009.0086
- Grellier, S., R. Guérin, H. Robain, A. Bobachev, F. Vermeersch, and A. Tabbagh. 2008. Monitoring of leachate recirculation in a bioreactor landfill by 2-D electrical resistivity imaging. *J. Environ. Eng. Geophys.* 13:351–359. doi:10.2113/JEEG13.4.351
- Grellier, S., K. Reddy, J. Gangathulasi, R. Adib, and C. Peters. 2006. Electrical resistivity tomography imaging of leachate recirculation in Orchard Hills Landfill. In: Proceedings of the Solid Waste Association of North America Conference, Charlotte, NC. Solid Waste Assoc. of North America, Silver Spring, MD. p. 1–7.
- Guérin, R., M.L. Munoz, C. Aran, C. Laperrelle, M. Hidra, E. Drouart, and S. Grellier. 2004. Leachate recirculation: Moisture content assessment by means of a geophysical technique. *Waste Manage.* 24:785–794. doi:10.1016/j.wasman.2004.03.010
- Gunn, D., J. Chambers, P. Hobbs, J. Ford, P. Wilkinson, G. Jenkins, and A. Merritt. 2013. Rapid observations to guide the design of systems for long-term monitoring of a complex landslide in the Upper Lias clays of North Yorkshire, UK. *Q. J. Eng. Geol. Hydrogeol.* 46:323–336. doi:10.1144/qjgeh2011-028
- Günther, T., C. Rücker, and K. Spitzer. 2006. Three-dimensional modelling and inversion of DC resistivity data incorporating topography: II. Inversion. *Geophys. J. Int.* 166:506–517. doi:10.1111/j.1365-246X.2006.03011.x
- Hilhorst, M. 2000. A pore water conductivity sensor. *Soil Sci. Soc. Am. J.* 64:1922–1925. doi:10.2136/sssaj2000.6461922x
- Hübner, R., T. Günther, K. Heller, U. Noell, and A. Kleber. 2017. Impacts of a capillary barrier on infiltration and subsurface stormflow in layered slope deposits monitored with 3-D ERT and hydro-metric measurements. *Hydrol. Earth Syst. Sci.* 21:5181–5199. doi:10.5194/hess-21-5181-2017

- Hübner, R., K. Heller, T. Günther, and A. Kleber. 2015. Monitoring hillslope moisture dynamics with surface ERT for enhancing spatial significance of hydrometric point measurements. *Hydrol. Earth Syst. Sci.* 19:225–240. doi:10.5194/hess-19-225-2015
- Intissar, R. 2009. Apport des méthodes électriques à la détermination de la structure interne d'une halde à stériles. M.S. thesis. Univ. of Montreal.
- Jayawickreme, D.H., R.L. Van Dam, and D.W. Hyndman. 2008. Subsurface imaging of vegetation, climate, and root-zone moisture interactions. *Geophys. Res. Lett.* 35:L18404. doi:10.1029/2008GL034690
- Johnson, T.C., G.E. Hammond, and X. Chen. 2017. PFLOTRAN-E4D: A parallel open source PFLOTRAN module for simulating time-lapse electrical resistivity data. *Comput. Geosci.* 99:72–80. doi:10.1016/j.cageo.2016.09.006
- Johnson, T.C., R.J. Versteeg, A. Ward, F.D. Day-Lewis, and A. Revil. 2010. Improved hydrogeophysical characterization and monitoring through parallel modeling and inversion of time-domain resistivity and induced-polarization data. *Geophysics* 75:WA27–WA41. doi:10.1190/1.3475513
- Kemna, A., J. Vanderborght, B. Kulesa, and H. Vereecken. 2002. Imaging and characterisation of subsurface solute transport using electrical resistivity tomography (ERT) and equivalent transport models. *J. Hydrol.* 267:125–146. doi:10.1016/S0022-1694(02)00145-2
- Kiflu, H., S. Kruse, M. Loke, P. Wilkinson, and D. Harro. 2016. Improving resistivity survey resolution at sites with limited spatial extent using buried electrode arrays. *J. Appl. Geophys.* 135:338–355. doi:10.1016/j.jappgeo.2016.10.011
- Koestel, J., R. Kasteel, A. Kemna, O. Esser, M. Javaux, A. Binley, and H. Vereecken. 2009. Imaging Brilliant Blue stained soil by means of electrical resistivity tomography. *Vadose Zone J.* 8:963–975. doi:10.2136/vzj2008.0180
- Koestel, J., A. Kemna, M. Javaux, A. Binley, and H. Vereecken. 2008. Quantitative imaging of solute transport in an unsaturated and undisturbed soil monolith with 3-D ERT and TDR. *Water Resour. Res.* 44:W12411. doi:10.1029/2007WR006755
- Kremer, T., C. Vieira, and A. Mainault. 2018. ERT monitoring of gas injection into water saturated sands: Modeling and inversion of cross-hole laboratory data. *J. Appl. Geophys.* 158:11–28. doi:10.1016/j.jappgeo.2018.06.001
- Kuras, O., J.D. Pritchard, P.I. Meldrum, J.E. Chambers, P.B. Wilkinson, R.D. Ogilvy, and G.P. Wealthall. 2009. Monitoring hydraulic processes with automated time-lapse electrical resistivity tomography (ALERT). *C. R. Geosci.* 341:868–885. doi:10.1016/j.crte.2009.07.010
- Kuras, O., P. Wilkinson, P. Meldrum, L. Oxby, S. Uhlemann, J. Chambers, et al. 2014. A trial of 4D cross-borehole electrical resistivity tomography (ERT) for detecting and monitoring subsurface leakage and contaminant transport, supporting the decommissioning of legacy silos at the Sellafeld site, UK. In: *Proceedings of the Waste Management Conference (WM2014)*, Phoenix, AZ. 2–6 Mar. 2014. WM Symposia, Tempe, AZ.
- Kuras, O., P.B. Wilkinson, P.I. Meldrum, L.S. Oxby, S. Uhlemann, J.E. Chambers, et al. 2016. Geoelectrical monitoring of simulated subsurface leakage to support high-hazard nuclear decommissioning at the Sellafeld Site, UK. *Sci. Total Environ.* 566–567:350–359. doi:10.1016/j.scitotenv.2016.04.212
- Lahmira, B., R. Lefebvre, M. Aubertin, and B. Bussièrè. 2017. Effect of material variability and compacted layers on transfer processes in heterogeneous waste rock piles. *J. Contam. Hydrol.* 204:66–78. doi:10.1016/j.jconhyd.2017.07.004
- Loke, M., J. Chambers, D. Rucker, O. Kuras, and P. Wilkinson. 2013. Recent developments in the direct-current geoelectrical imaging method. *J. Appl. Geophys.* 95:135–156. doi:10.1016/j.jappgeo.2013.02.017
- Loke, M., H. Kiflu, P. Wilkinson, D. Harro, and S. Kruse. 2015a. Optimized arrays for 2D resistivity surveys with combined surface and buried arrays. *Near Surf. Geophys.* 13:505–517.
- Loke, M., P. Wilkinson, J. Chambers, and M. Strutt. 2014a. Optimized arrays for 2D cross-borehole electrical tomography surveys. *Geophys. Prospect.* 62:172–189. doi:10.1111/1365-2478.12072
- Loke, M., P. Wilkinson, J. Chambers, S. Uhlemann, and J. Sorensen. 2015b. Optimized arrays for 2-D resistivity survey lines with a large number of electrodes. *J. Appl. Geophys.* 112:136–146. doi:10.1016/j.jappgeo.2014.11.011
- Loke, M., P. Wilkinson, S. Uhlemann, J. Chambers, and L. Oxby. 2014b. Computation of optimized arrays for 3-D electrical imaging surveys. *Geophys. J. Int.* 199:1751–1764. doi:10.1093/gji/ggu357
- Martin, V., M. Aubertin, B. Bussièrè, and P. Chapuis. 2004. Evaluation of unsaturated flow in mine waste rock. In: *Proceedings of the 57th Canadian Geotechnical Conference with the 5th joint CGS-IAH Conference*, Quebec, QC, Canada. 24–26 Oct. 2004. Can. Geotech. Soc., Alliston, ON.
- Martin, V., M. Aubertin, G. Zhan, B. Bussièrè, and R. Chapuis. 2006. Investigation into the hydrological behavior of exposed and covered waste rock dumps. *Trans. Soc. Min. Metall. Explor.* 318:139–146.
- Martin, V., B. Bussièrè, B. Plante, T. Pabst, M. Aubertin, F. Medina, et al. 2017. Controlling water infiltration in waste rock piles: Design, construction, and monitoring of a large-scale in-situ pilot test pile. In *Proceedings of the 70th Canadian Geotechnical Society Conference: 70 Years of Canadian Geotechnics and Geoscience, GeoOttawa 2017*, Ottawa, ON. 1–4 October 2017. Can. Geotech. Soc., Alliston, ON.
- McCarter, M., 1990. Design and operating considerations for mine waste embankments. In: B.A. Kennedy, editor, *Surface mining*. 2nd ed. Soc. Min., Metall., Explor., Littleton, CO. p. 890–899.
- McLemore, V.T., A. Fakhimi, D. van Zyl, G.F. Ayakwah, K. Anim, K. Boakye, et al. 2009. Literature review of other rock piles: Characterization, weathering, and stability. New Mexico Bureau of Geology and Mineral Resources, Open-file Rep. OF-517. New Mexico Inst. Min. Technol., Socorro.
- Michot, D., Y. Benderitter, A. Dorigny, B. Nicoullaud, D. King, and A. Tabbagh. 2003. Spatial and temporal monitoring of soil water content with an irrigated corn crop cover using surface electrical resistivity tomography. *Water Resour. Res.* 39:1138. doi:10.1029/2002WR001581
- Molson, J.W., O. Fala, M. Aubertin, and B. Bussièrè. 2005. Numerical simulations of pyrite oxidation and acid mine drainage in unsaturated waste rock piles. *J. Contam. Hydrol.* 78:343–371. doi:10.1016/j.jconhyd.2005.06.005
- Morin, K.A. 1990. Critical literature review of acid drainage from waste-rock. MEND/NEDEM Rep. 1.11.1. Can. Ctr. for Mineral and Energy Technology.
- Nimmer, R.E., J.L. Osiensky, A.M. Binley, and B.C. Williams. 2008. Three-dimensional effects causing artifacts in two-dimensional, cross-borehole, electrical imaging. *J. Hydrol.* 359:59–70. doi:10.1016/j.jhydrol.2008.06.022
- Ogilvy, R., P. Meldrum, O. Kuras, P. Wilkinson, J. Chambers, M. Sen, et al. 2009. Automated monitoring of coastal aquifers with electrical resistivity tomography. *Near Surf. Geophys.* 7:367–375.
- Peregoedova, A., M. Aubertin, B. Bussièrè. 2013. Laboratory measurement and prediction of the saturated hydraulic conductivity of mine waste rock. In: *Proceedings of the GeoMontreal 2013: Geoscience for Sustainability*, Montreal, QC, Canada. 29 Sept.–3 Oct. 2013. Can. Geotech. Soc., Alliston, ON.
- Plante, B., M. Benzaazoua, and B. Bussièrè. 2011a. Predicting geochemical behaviour of waste rock with low acid generating potential using laboratory kinetic tests. *Mine Water Environ.* 30:2–21. doi:10.1007/s10230-010-0127-z
- Plante, B., M. Benzaazoua, and B. Bussièrè. 2011b. Kinetic testing and sorption studies by modified weathering cells to characterize the potential to generate contaminated neutral drainage. *Mine Water Environ.* 30:22–37. doi:10.1007/s10230-010-0131-3
- Plante, B., M. Benzaazoua, B. Bussièrè, M. Biesinger, and A. Pratt. 2010. Study of Ni sorption onto Tio mine waste rock surfaces. *Appl. Geochem.* 25:1830–1844. doi:10.1016/j.apgeochem.2010.09.010
- Plante, B., B. Bussièrè, and M. Benzaazoua. 2014. Lab to field scale effects on contaminated neutral drainage prediction from the Tio mine waste rocks. *J. Geochem. Explor.* 137:37–47. doi:10.1016/j.gexplo.2013.11.004
- Poaty, B., B. Plante, B. Bussièrè, M. Benzaazoua, T. Pabst, M. Aubertin, et al. 2018. Geochemical behavior of different waste rock configurations from the Lac Tio mine: Comparison between column tests and experimental waste rock pile results. In: *Proceedings of Tailings and Mine Waste Conference*, Keystone, CO. 30 Sept.–2 Oct. 2018. p. 811–821.
- Poisson, J., M. Chouteau, M. Aubertin, and D. Campos. 2009. Geophysical experiments to image the shallow internal structure and the moisture

- distribution of a mine waste rock pile. *J. Appl. Geophys.* 67:179–192. doi:10.1016/j.jappgeo.2008.10.011
- Power, C., J.I. Gerhard, M. Karaoulis, P. Tsourlos, and A. Giannopoulos. 2014. Evaluating four-dimensional time-lapse electrical resistivity tomography for monitoring DNAPL source zone remediation. *J. Contam. Hydrol.* 162–163:27–46. doi:10.1016/j.jconhyd.2014.04.004
- Power, C., P. Tsourlos, M. Ramasamy, A. Nivorlis, and M. Mkandawire. 2018. Combined DC resistivity and induced polarization (DC-IP) for mapping the internal composition of a mine waste rock pile in Nova Scotia, Canada. *J. Appl. Geophys.* 150:40–51. doi:10.1016/j.jappgeo.2018.01.009
- Robinson, D., C. Campbell, J. Hopmans, B.K. Hornbuckle, S.B. Jones, R. Knight, et al. 2008. Soil moisture measurement for ecological and hydrological watershed-scale observatories: A review. *Vadose Zone J.* 7:358–389. doi:10.2136/vzj2007.0143
- Robinson, D., I. Lebron, B. Kocar, K. Phan, M. Sampson, N. Crook, and S. Fendorf. 2009. Time-lapse geophysical imaging of soil moisture dynamics in tropical deltaic soils: An aid to interpreting hydrological and geochemical processes. *Water Resour. Res.* 45:W00D32. doi:10.1029/2008WR006984
- Rücker, C., T. Günther, and K. Spitzer. 2006. Three-dimensional modelling and inversion of dc resistivity data incorporating topography: I. Modelling. *Geophys. J. Int.* 166:495–505. doi:10.1111/j.1365-246X.2006.03010.x
- Rücker, C., T. Günther, and F.M. Wagner. 2017. pyGIMLI: An open-source library for modelling and inversion in geophysics. *Comput. Geosci.* 109:106–123. doi:10.1016/j.cageo.2017.07.011
- Rucker, D.F., J.B. Fink, and M.H. Loke. 2011. Environmental monitoring of leaks using time-lapsed long electrode electrical resistivity. *J. Appl. Geophys.* 74:242–254. doi:10.1016/j.jappgeo.2011.06.005
- Scaini, A., M. Audebert, C. Hissler, F. Fenicia, L. Gourdol, L. Pfister, and K.J. Beven. 2017. Velocity and celerity dynamics at plot scale inferred from artificial tracing experiments and time-lapse ERT. *J. Hydrol.* 546:28–43. doi:10.1016/j.jhydrol.2016.12.035
- Singha, K., F.D. Day-Lewis, T. Johnson, and L.D. Slater. 2015. Advances in interpretation of subsurface processes with time-lapse electrical imaging. *Hydrol. Processes* 29:1549–1576. doi:10.1002/hyp.10280
- Singha, K., and S.M. Gorelick. 2005. Saline tracer visualized with three-dimensional electrical resistivity tomography: Field-scale spatial moment analysis. *Water Resour. Res.* 41:W05023. doi:10.1029/2004WR003460
- Slater, L., A. Binley, W. Daily, and R. Johnson. 2000. Cross-hole electrical imaging of a controlled saline tracer injection. *J. Appl. Geophys.* 44:85–102. doi:10.1016/S0926-9851(00)00002-1
- Smith, L.J., M.C. Moncur, M. Neuner, M. Gupton, D.W. Blowes, L. Smith, and D.C. Segó. 2013. The Diavik Waste Rock Project: Design, construction, and instrumentation of field-scale experimental waste-rock piles. *Appl. Geochem.* 36:187–199. doi:10.1016/j.apgeochem.2011.12.026
- Stummer, P., H. Maurer, and A.G. Green. 2004. Experimental design: Electrical resistivity data sets that provide optimum subsurface information. *Geophysics* 69:120–139. doi:10.1190/1.1649381
- Uhlemann, S., J. Chambers, P. Wilkinson, H. Maurer, A. Merritt, P. Meldrum, et al. 2017. Four-dimensional imaging of moisture dynamics during landslide reactivation. *J. Geophys. Res. Earth Surf.* 122:398–418. doi:10.1002/2016JF003983
- Uhlemann, S., A. Smith, J. Chambers, N. Dixon, T. Dijkstra, E. Haslam, et al. 2016a. Assessment of ground-based monitoring techniques applied to landslide investigations. *Geomorphology* 253:438–451. doi:10.1016/j.geomorph.2015.10.027
- Uhlemann, S., J. Sorensen, A. House, P. Wilkinson, C. Roberts, D. Goody, et al. 2016b. Integrated time-lapse geoelectrical imaging of wetland hydrological processes. *Water Resour. Res.* 52:1607–1625. doi:10.1002/2015WR017932
- Uhlemann, S., P.B. Wilkinson, H. Maurer, F.M. Wagner, T.C. Johnson, and J.E. Chambers. 2018. Optimized survey design for electrical resistivity tomography: Combined optimization of measurement configuration and electrode placement. *Geophys. J. Int.* 214:108–121. doi:10.1093/gji/ggy128
- Wilkinson, P.B., M.H. Loke, P.I. Meldrum, J.E. Chambers, O. Kuras, D.A. Gunn, and R.D. Ogilvy. 2012. Practical aspects of applied optimized survey design for electrical resistivity tomography. *Geophys. J. Int.* 189:428–440. doi:10.1111/j.1365-246X.2012.05372.x
- Wilkinson, P., P. Meldrum, O. Kuras, J. Chambers, S. Holyoake, and R. Ogilvy. 2010. High-resolution electrical resistivity tomography monitoring of a tracer test in a confined aquifer. *J. Appl. Geophys.* 70:268–276. doi:10.1016/j.jappgeo.2009.08.001
- WSP Canada. 2014. Management of waste rocks and water at the Lac Tio mine. WSP Canada, Trois-Rivières, QC.